COMPUTATION OF EROSIVE BURNING RATE OF FLAT COMPOSITE PROPELLANT GRAIN

by

DINESH KUMAR KAUSHIK

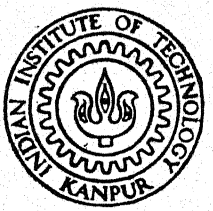

DEPARTMENT OF AEROSPACE ENGINEERING

INDIAN INSTITUTE OF TECHNOLOGY, KANPUR

AUGUST, 1990

COMPUTATION OF EROSIVE BURNING RATE OF FLAT COMPOSITE PROPELLANT GRAIN

A Thesis Submitted
in Partial Fulfilment of the Requirements
for the Degree of

MASTER OF TECHNOLOGY

by

DINESH KUMAR KAUSHIK

to the

DEPARTMENT OF AEROSPACE ENGINEERING

INDIAN INSTITUTE OF TECHNOLOGY, KANPUR

AUGUST, 1990

AE - 1990 - M - KAV - COM

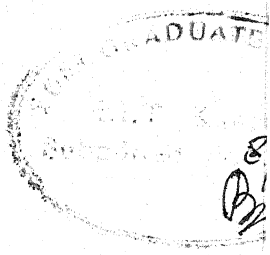

CERTIFICATE

This is to certify that the work for the thesis entitled, " Computation of Erosive Burning Rate of Flat Composite Propellant Grain " , has been carried out by Mr. Dinesh Kumar Kaushik (Roll No. 8810105) under my supervision and that it has not been submitted elsewhere for a degree.

O P Sharma

(Dr. O.P.SHARMA),

Professor,

Dept. Of Aerospace Engg. ,

Indian Institue of Technology ,

Kanpur – 208 016 .

ACKNOWLEDGEMENTS

I wish to express my sincere thanks to my thesis supervisor, Dr. O. P. Sharma, for suggesting me this problem and valuable guidance throughout the course of this work.

I also thank all my friends here in I. I. T. Kanpur , particularly S. Chojar, C. V. K. Singh, Prabhu and Srinivasan, for giving me encouragement and helping me to complete this work in time.

DINESH K. KAUSHIK

ABSTRACT

The burning rate of a composite solid propellant is affected by the cross— flow. of combustion gases. This phenomenon is called erosive burning. In this .ork, erosive burning of composite solid propellant is investigated by a steady, two - dimensional, chemically reacting, turbulent boundary layer over a propellant surface The turbulence is modelled through the much used two equation (k - ε) model while Spalding's Eddy Break - Up model is employed to model the gas phase reaction ~~model~~. The method used to solve the boundary layer equations is due to Patankar and Spalding. This is a semi - implicit finite difference scheme in which the conservation equations (transformed in x ~ ω coordinates) are integrated over the control volumes constituting the boundary layer while marching in x - direction.

The increase in free stream velocity brings the location of peak heat release zone closer to the propellant surface, thus, increasing its burning rate Also, the effect of normal burning rate, particle size and ,surface roughness height is investigated.

CONTENTS

NOMENCLATURE

A_g = Arrehenius Frequency Factor in gaseous phase reactions, $(m^3)^{n-1} s^{-1} (kmole)^{1-n}$

A_s = Arrehenius Frequency factor in propellant surface decomposition, m/s

C_p = Average specific heat capacity of reacting gases, kcl/kg-K

C_s = Heat capacity of solid propellant, kcal/kg-K

D = Diffusion coefficent of Fick's Law, m^2/s

E_{ag} & E_{as} = Activation Energies in the gas phase reaction and propellant surface decomposition, Kcal/mole.

ω = Non dimensional Stream function

H = Total enthalpy of gases, kacl/kg

λ = Thermal Conductivity of the gas, kcal/m-s-K

n = Order of chemical reaction

P = Pressure, N/m^2

P_r = Molecular Prandtl Number, $\mu C_p/\lambda$

P_{rt} = Turbulent Prandtl Number.

Q_s = Net heat release at the surface per unit mass, kcal/kg

r_b = Total burning rate of the solid propellant, m/s.

r_{bo} = Strand burning rate of the solid propellant, m/s

R_x = Reynold's Number based on x

R_u = Universal Gas Constant, N-m/kmole-K

S_c = Molecular Schmidt Number, $\mu/\rho D$

S_{ct} = Turbulent Schmidt Number

T = Temperature, ^0K

T_p = Propellant Temperature, ^0K

T_{pi} = Propellant initial Temperature, ^0K

T_{ps} = Propellant surface Temperature, ^0K

$\bar{T}_{ps}$ = Reference Propellant surface Temperature, ^0K

$\bar{u}$ = Gas velocity in the x direction, m/s

u_e = Free stream velocity, m/s

U_τ = Friction Velocity, m/s

$\bar{v}$ = Gas velocity in the y direction, m/s

$\dot{w}_i$ = Rate of production of species i due to reaction, kg/m^3s

W = Average molecular weight of gases, kg/mole

W_O, W_F = Molecular Weight of oxidizer, fuel, kg/mole.

x = Coordinate in the x direction

y = Coordinate in the y direction

Y_i = Mass fraction of the species, i

Y_{FS} = Mass fraction of the fuel in the composite solid propellant

Y_{OS} = Mass fraction of the oxidizer in the composite solid propellant

μ_t = Eddy (turbulent) viscosity

ω = coordinate along the direction normal to the propellant surface

ψ = Stream function

λ_s = Thermal conductivity of solid propellant, kcal/m-s-K

μ = Gas viscosity, kg/m-s

ρ = Gas density, kg/m^3

ρ_s = Solid propellant density, kg/m^3

ν_o, ν_F = Stochiometric Coefficents of oxidizer and fuel

Subscripts

∞ = Free stream values

F = Represents the fuel specie in the reaction

i = Species index representing any of the species in chemcial reactions,

o = Represents the oxidizer specie in the reaction

w = Wall values

$\bar{(\ )}$ = Averaged Quantities

$(\ )'$ = Fluctuating Quantities

$\tilde{(\ )}$ = Mass-Weighted Average

List of Figures

Chapter 1 | Introduction

(1.a) General

When a solid prepellant burns in the presence of crossflow of combustions gases, its burning rate is affected In the absence of a crossflow, burning rate of a composite propellant depends on the chamber pressure, initial propellant temperature, fuel to oxidiser ratio, propellant configuration and oxidiser particle size. But in the presence of a crossflow, after a threshold velocity is reached, burning rate becomes a strong function of velocity & usually increases with velocity (other paramers remaining fixed) This phenomenon is called erosive burning.

High performance rockets require high thrust and short burning time which in twin require high volumetric loading fractions High loading fractions result in low part to length ratios and this means that crossflow velocity becomes high enough resulting in erosive burning. This may give rise to unequal propellant-web burnout, early exposure of the part of the rocket motor casing to the hot combustion products and overpressurization immediately following ignition. So erosive burning effect needs to be accounted seriously shile designing the grain and rocket motor. The phenomenon of erosive burning has also received a considerable attention because of nozzless rocket motors (which offer significant economic advantage & simplicity over conventional motors). Here gases reach sonic & supersonic velocities over the grain surface leading to high erosive burning rates.

(1.b) Background of the Problem

As repored by Von Braun, erosive burning studies of solid propellants were made in many countries like Germany, Japan, Britain, USSR etc and date back as early as 1889 The erosive burning effect was observed by Mansel on cordite. Muraour was probably the first investigator to describe the erosive phenomenon explicity (Ref. (1)).

Over the years, a large number of erosive burning models have been reported. Generally these models differ in the physical basis attributed as a reason for enhancement of the burning rate with increase in velocity Exhaustive literature reviews on erosive burning problem are published by King[2] and Kuo and Razdan[1] Some of the recent models relevant for the present work are reviewed here in brief.

Lenoir and Robillard[3] developed their model on the premise that erosive burning is driven by increased heat transfer from the mainstream gas flow associated with increased heat transfer coefficient with increased mass flux parallel to the grain surface. They calculated the total burning rate (r_b) as the sum of the normal burning rate (r_{bo}) and a second erosive term resulting from heat transfer from the core flow to the propellant surface i e

$$r_b = r_{bo} + r_{be} \qquad (1.1)$$

In this equation it is presumed that the pressure-dependent normal burning rate r_{bo} is unaffected by an increase in total rate at a given pressure. Also r_{be} is postulated to be proportional to heat transfer coefficient This model has been widely used due to its simiplicity but the additive assumption (1.1) is disputed

and is still not resolved.

A model of composite propellant combustion was presented by Hermance[4] He considers the combustion problem on a sufficiently broad scale to be free of empirically derived constants. But he assumed a very unrealistic assumption about propellant surface a heterogeneous reaction is assumed to occur in a cusp between the oxidiser crystals and the binder, the cusp resulting from the spherical regression of the oxidiser particles Recent studies of extinguished surfaces by Boggs and others have shown these assumptions to be invalid

Another somewhat more advanced combustion model was put forward by Beckstead, Derr and Price[5] This model is based on a flame structure surrounding individual oxidizer crystals Three separate flame zones are considered

(1) A primary flame between the decomposition products of tthe binder and the oxidizer

(2) A premixed oxidiser flame

(3) A final diffusion flame between the products of the other two flames

The oxidizer decomposition is taken as being the over-all controlling factor in the combustion process. The results obtained matched excellentally with experimental trends in the case of surface temperature and the effect of oxidizer concentration. But the predicted effect of particle size is somewhat greater than observed experimentally

King[2] has based his model of erosive burning on the convective

bending of the diffusion-controlled flame zone As the total combustion length scale is assumed constant, the resulting flame zone lies closer to the propellant surface and provides increased heat transfer He has criticized the Lenoir-Robillard theory in the light of experimental evidence, as L-R model predicts a strong dependence of burning rate on the core gas temperature But King's flame bending model is found to underpredict the erosive burning effects severely

In Lengelle's model[6], the basic propellant combustion mechanism is the granular diffusion model in which pockets of fuel vapour leave the surface and burn away in an oxidizer continuum at a rate strongly dependent upon the rate of micro mixing of the oxidiser vapour into the fuel vapour pocket The effect of crossflow is assumed to be associated with the increase in turbulence with increasing crossflow raising the turbulent diffusivity in the mixing region (thus increasing rate of mixing of binder and oxidiser product gases) and raising the effective turbulent thermal conductivity, which, in turn, increases the heat transfer rate from the flame to the surface Lengelle has ignored the ammonium perchlorate monopropellant flame. Also in his treatment of boundary layer, he has used the power velocity law all the way from the freestream to the surface on the groound that since this law is valid upto "inner zone" of the boundary layer and gradients are steeper near the surface, this velocity law can be extended right upto the freetream. But this is an oversimplification of the problem in a bid to get a simple final expression for the burning rate.

The objective of Beddini's model[7] is to investigate the role of turbulence in erosive burning. His flow field analysis is coupled with a simple

model of propellant combustions in which the mass burning rate is assumed to be directly proportional to the heat flux from the gas to the surface and the gas phase reaction is assumed to be described as a single-step homogeneous reaction, with no consideration of the heterogeity of flame structure associated with composite propellants

Kuo and Razdan[8] used a second order closure model for characterisation of the flow field in erosive burning situations , the closure model (k-ε model) being used differing from that being used by Beddini They have used Spalding's Eddy Breakup Model for modeling the gas phase chemical reactions They concluded that propellants with lower normal burning rates are more sensitive to erosive burining and rate of burning increases with surface roughness

Renie and Osborn[9] presented a mathematical model for determining the erosive burning rate. The physical reason attributed to erosive burning effect is same as of Lengelle that this phenomenon is due to an increase in the value of the transport properties in the gas phase reaction zone caused by the presence of a turbulent boundary layer. They have coupled a unique statistical combustion model, the petite ensemble model (PEM). They have also incorporated a turbulence model based on mixing length hypothesis as modified for surface roughness by Cebeci & Chang[14] . They have predicted the effects of cross-flow velocity, base burning rate, pressure and surface roughness on the erosive burning sensitivity.

One recent model is due to Godon, Duterque and Lengelle[10] They

have solved Navier-Stokes equations numerically, simplified with the shear flow approximation and for a two dimensional flow. Near the wall, they have applied couette flow approximation. They also use a mixing length closure model. In the "wall zone", they have obtained a flame height criterion by considering that the combustion is limited essentially by the diffusion between oxidising and fuel gases. Both the flow description and erosive burning are sucessfully compared with experimental results: cold flow-porous wall simulation with laser anemometry measured velocity profiles and propellants erosive burning measured with an ultrasonic transducer on a separated generator sample device. They have very clearly predicted the effect of particle size, existence of threshold velocity and effect of normal burning rate.

A very recent model presented by Sabnis, Gibeling and McDonald[11] employs a multi dimensional implicit Navier-Stokes analysis. Most of the models which we have discussed used boundary-layer approximation to describe the flow field. In a number of instances, such as the flow in the region of inhibiters, slots and submerged nozzles, the boundary layer approximations are not valid. In the present model, ensemble-averaged Navier-Stokes equations for a cylindrical coordinate system are applied to the simulation of the steady mean flow in rocket motor chambers. They have used a two equation turbulence (k-ε) model. The computed results show good agreement with the experimental data from cold-flow experiments on the axial velocity profiles. Also the axial location of transition to turbulent flow is predicted reasonably well.

(1.c) Physical Basis of Erosive Burning Phenomenon

While reviewing the work of different researcher in the previous section, we noticed three different reasons responsible for enhancementt of burning rate with crooss-stream velocity

(i) Heat transfer from a "core" gas to the propellant surface by forced convection

(ii) Convective bending of the diffusion-controlled flame zone.

(iii) Enhancement of transport properties in the gas phase reaction zone by cross-flow induced turbulence.

The first factor , if taken as a basis for erosive burning phenomenon, predicts a strong depends of erosive burning rate on the core gas temperature which is widely criticized in literature (Ref 2,7 & 9).

The second factor underpredicts the burning rate severely (see Ref.2) , therefore, can't be accepted as a reasonable basis for erosive burning problem

The third factor, in fact, is the most agreed upon basis for erosive burning phenomenon and many researchers (see Ref.6-11) have developed their models with this as a reason for erosive effects. Kuo and Razdan[8] quite clearly showed that turbulence does affect the burning rate quite strongly Increase in free-stream velocity brings the location of the peak turbulent intensity closer to the propellant surface, which means that the turbulence eddies with high frequencies come closer to the propellant surface. This causes an increase in the mixing rate of oxidiser and fuel species, therefore, increasing the gas phase

reaction rate

In this work also, this is the third factor, which is considred the physical basis for erosive burning phenomenon.

(1 d) Modelilng Approach

As already stated, erosive burning phenomenon is observed as a result of the interaction between fluid freestream velocity and the combustion process. Any attempt towards erosive burning modeling should be started with integrating a fluid mechanical analysis with a combustion mechanism. In fact, it is the surface temperature which provides the link between the burning rate and the gas dynamics In this work also, the approach is similar and we can articulate the calculation procedure in the following words. (i) calculate heat flux from gas to solid phase by showing the gas-phase conservation equations & thus determine the propellant surface temperature and (ii) utilize the knowledge of surface temperature to calculate the burning rate.

An acceptable model must account for the physically observed facts about erosive burning phenomenon in (i) a trendwise way (ii) quantitative way. A few common observations of importance from the past experimental studies are enlisted below

(i) Plots of burning rate versus gas velocity or mass flux at constant pressure are not fitted best by a straight line.

(ii)There is a threshold velocity below which erosive effects are not observed. Also higher the pressure, lower is the value of threshold velocity.

(iii) Slower burning propellants are more strongly affected by crossflows than higher burning propellants

(iv) Small particle size AP monopropellants are less affected by the cross flow while the large particle size are affected tremendously.

(v) At high velocities, erosive effects enhance with increase in surface roughness

In this work, objective has been (1) to calculate erosive burning rate from an aerothermochemical analysis for a composite propellant (2) to examine whether the theoretical model meets the test of observation or not. by comparing the results with the above-stated facts from experimental studies.

Chapter 2 | Formulation Of The problem

(2 a) Description of the Model

In this work, an aerothermochemical analysis to erosive burning problem is presented in terms of two equation model (k - ε) for turbulence[16-17] and Spalding's eddy break-up (EBU)[13] model for combustion process, which considers the heat, mass and momentum transfer in a chemically reacting turbulent boundary layer.

Hot gases flow over two dimensional slab of propellant and form a boundary layer on it (Fig. 1). To analyse the flowfield, where the heat and mass transfer is taking place between the boundary layer and the propellant surface, we make the following assumptions:

(i) The boundary layer is two dimensional, quasisteady and chemically reacting

(ii) The flowfield is statistically stationary i.e. each instantaneous variable can be replaced by its mean and fluctuating part.

(iii) Body forces are absent

(iv) There is no radiative heat transfer.

(v) The Lewis number is unity.

(vi) Fick's law of diffusion is valid.

(vii) $\dfrac{\overline{\mu' \dfrac{\partial u}{\partial y}}}{\mu \dfrac{\partial \bar{u}}{\partial y}} \ll 1$ and $\dfrac{\overline{\rho' u' v'}}{\bar{\rho}\, \overline{u'v'}} \ll 1$

In each case, these ratios can be assumed to be less than 5% for Mach numbers

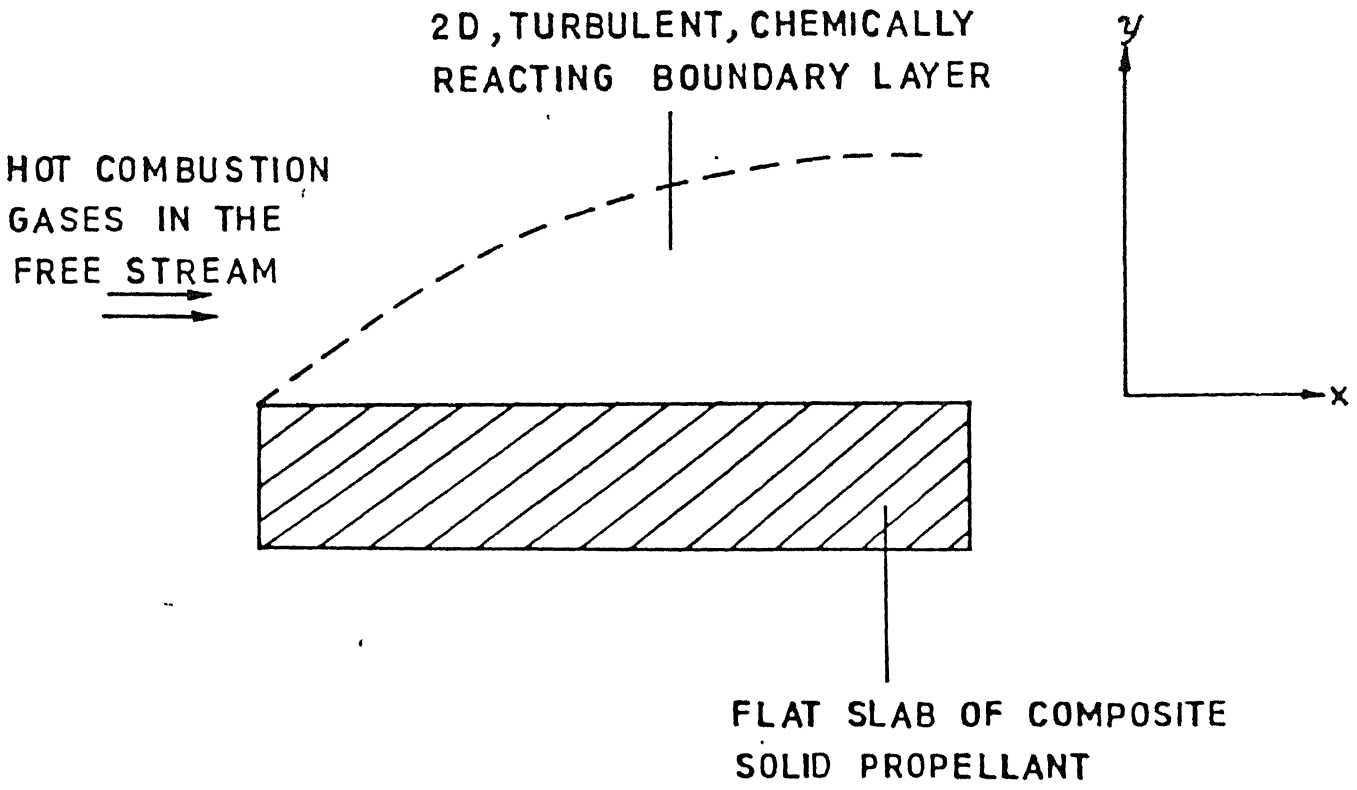

FIG.1 SCHEMATIC REPRESENTATION OF THE PHYSICAL MODEL

less than 5. If the correlations between viscosity and velocity gradient and between density and $u'v'$ fluctuations are at the most 0.3, a conservative estimate (Ref. 19, p. 73).

(viii) There is no reaction-generated turbulence.

Starting with the general conservation equations for a reacting compressible flow, we get the following simplified form of conservation equations, by doing an order of magnitude analysis combined with the above set of assumptions (See Ref. 18, Ch.9 and Ref. 19, Ch.3 for details).

(i) Continuity Equation :

$$\frac{\partial}{\partial x}\left(\bar{\rho}\,\bar{u}\right) + \frac{\partial}{\partial y}\left(\bar{\rho}\,\bar{v}\right) = 0 \qquad (2.1)$$

(ii) X-Momentum Equation :

$$\bar{\rho}\,\bar{u}\frac{\partial \bar{u}}{\partial x} + \bar{\rho}\,\bar{v}\frac{\partial \bar{u}}{\partial y} = -\frac{d\bar{p}}{dx} + \frac{\partial}{\partial y}\left[\mu_{eff}\ \frac{\partial \bar{u}}{\partial y}\right] \qquad (2.2)$$

(iii) Species conservation Equation :

$$\bar{\rho}\,\bar{u}\frac{\partial \bar{Y}_i}{\partial x} + \bar{\rho}\,\bar{v}\frac{\partial \bar{Y}_i}{\partial y} = \frac{\partial}{\partial y}\left[\left(\frac{\mu}{Sc}\right)_{eff}\ \frac{\partial \bar{Y}_i}{\partial y}\right] + \bar{\omega}_i$$

where, i = F, for fuel (2.3a)

= O, for oxidiser (2.3b)

But the species consevation equations are solved for $\bar{Y}_F$ and $\bar{Y}_{OF}$ (Eq.2.3b) where

$$\bar{Y}_{OF} = \bar{Y}_O - \frac{\nu_O W_O}{\nu_F W_F}\,\bar{Y}_F$$

This choice of variable eliminates the non-linear term in the equation for this variable. Also no separate conservation equation equation is needed for the product species as $\bar{Y}_P = (1 - \bar{Y}_F - \bar{Y}_O)$.

(iv) Energy Equation :

$$\bar{\rho}\,\bar{u}\frac{\partial \bar{H}}{\partial x} + \bar{\rho}\,\bar{v}\frac{\partial \bar{H}}{\partial y} = \frac{\partial}{\partial y}\left\{\left(\frac{H}{Pr}\right)_{eff}\frac{\partial \bar{H}}{\partial y} + \left[\mu_{eff} - \left(\frac{\mu}{Pr}\right)_{eff}\right]\frac{\partial \bar{u}^2}{\partial y}\right\} \qquad (2.4)$$

(v) Equation of State :

$$\bar{\rho} = \frac{\bar{\rho}\, R^{\circ}\, \bar{T}}{W} \tag{2·5}$$

For various correlation terms, we have used the following correlations

(i) Reynolds Stress $\overline{u'v'}$ is related to turbulent viscosity by the following equation

$$-\bar{\rho}\,\overline{u'v'} = \mu_t \frac{\partial \bar{u}}{\partial y} \tag{2·6}$$

Thus $\mu_{eff} = \mu + \mu_t$

(ii) Mass transfer by turbulent diffusion , that is , $\overline{(\rho\, v)'\, Y_i'}$ is modelled in the following way

$$-\overline{(\rho v)'\, Y_i'} = \frac{\mu_t}{Sc_t} \frac{\partial \bar{Y}_i}{\partial y} \tag{2·7}$$

(iii) Heat transfer , $\overline{(\rho\, v)'\, h_i'}$ is modelled by using Reynold's analogy ,

$$-\overline{(\rho v)'\, h_i'} = \frac{\mu_t}{Pr_t} \frac{\partial \bar{h}_i}{\partial y} \tag{2·8}$$

(2 b) Turbulence Model

For closure of the above stated problem , a two equation model of turbulence is used in this work . This model characterises turbulence by turbulent kinetic energy ($k \equiv \frac{\overline{u_i'\, u_i'}}{2}$) and its dissipation rate ($\varepsilon \equiv \mu \frac{\overline{u_{i,j}'\, u_{i,j}'}}{\bar{\rho}}$) The (k - ε) model was originally developed by Harlow and Nakayama (Ref 11) and was subsequently improved by many researchers Here , k-ε model due to Launder and Spalding[16] is utilized .The potential advantage of such a transport model is that it is capable of characterising a turbulent flow adequately without specification of the length scale required by mixing-length models

The turbulent kinetic energy equation for a steady , two-dimensional boundary layer flow can be written as (see Ref 8)

$$\bar{\rho}\,\bar{u}\,\frac{\partial k}{\partial x} + \bar{\rho}\,\tilde{v}\,\frac{\partial k}{\partial y} = \frac{\partial}{\partial y}\left[\left(\mu + \frac{\mu_t}{C_1}\right)\frac{\partial k}{\partial y}\right] + \mu_t\left(\frac{\partial \bar{u}}{\partial y}\right)^2 - \bar{\rho}\,\varepsilon \qquad (2\cdot9)$$

The form of ε-equation[16] is as applicable to uniform property flow . However , we modify it by retaining the full expression for the production of k , that is , the second term on the right hand side of k-equation The ε-equation for a steady , two-dimensional , boundary layer flow is (see Ref. 8)

$$\bar{\rho}\,\bar{u}\,\frac{\partial \varepsilon}{\partial x} + \bar{\rho}\,\tilde{v}\,\frac{\partial \varepsilon}{\partial y} = \frac{\partial}{\partial y}\left[\left(\mu + \frac{\mu_t}{C_2}\right)\frac{\partial \varepsilon}{\partial y}\right] + C_3\,\mu_t\left(\frac{\partial \bar{u}}{\partial y}\right)^2\frac{\varepsilon}{k} - C_4\,\bar{\rho}\,\frac{\varepsilon^2}{k} \qquad (2\cdot10)$$

While solving Eqns. (2.9) and (2.10) , the influence of nearby wall is considered by means of widely used wall-function method (see Ref 16 for details) The turbulent viscosity μ_t is related to k and ε by the following relation ,

$$\mu_t = C_\mu\,\frac{\bar{\rho}k^2}{\varepsilon} \qquad (2\cdot11)$$

(2.c) Gas - Phase Reaction Model

In the boundary layer above a burning composite propellant , gases may react in several steps , but in the present work , a single - step global forward reaction is assumed :

$$\nu_F F + \nu_O O \rightarrow \nu_P P \qquad (2\cdot12)$$

For such a reaction , the following Arrhenius type expression for the global reaction rate for fuel species is used ,

$$\dot{\omega}_F = -\,W_F\,k_g\left(\frac{\rho\,Y_F}{W_F}\right)^{\nu_F}\left(\frac{\rho\,Y_O}{W_O}\right)^{\nu_O} \qquad (2\cdot13)$$

where , $$k_g = A_g\,e^{-\frac{E_{ag}}{R_u T}} \qquad (2\cdot14)$$

In species conservation equation (2.3) , we need to know average value of reaction rate , $\overline{\omega_F}$ ($\overline{\omega_O}$ can be eliminated by the choice of variable , OF, as discussed earlier) In this work Spalding's Eddy Break-Up (EBU) model is utilized to derive an expression for $\overline{\omega_F}$. In this model , it is proposed that the gases in a turbulent flame , at high Reynolds numbers , should be considered as lumps or eddies of unburned and fully burned gases. The rate of burning depends the rate at which fragments of unburned gases are broken into still smaller fragments by the action of turbulence.

The EBU concept can be used to model the gas - phase reaction rate for erosive burning problem The fuel and oxidiser gases are unmixed as they come out of the propellant surface.The presence of high lateral gradients in the boundary layer creates the turbulent eddies. It is reasonable to assume that these eddies engulf fuel and oxidiser gases , thus giving rise to fuel and oxidiser eddies

Applying the EBU concept further , it turns out that in a diffusion controlled reaction , the rate of consumption of fuel is proportional to the dissipation rate of fuel containing eddies , characterized by ($\bar{\rho}\sqrt{\overline{Y_F'^2}} \cdot \frac{\varepsilon}{k}$) , where $\frac{\varepsilon}{k}$ is the turbulent time scale. So , we can write ,

$$\dot{\omega}_F \propto - \bar{\rho}\sqrt{\overline{Y_F'^2}} \cdot \frac{\varepsilon}{k} \quad . \tag{2.15}$$

If we further assume that in the conservation equation for $\overline{Y_F'^2}$, only the production and dissipation terms are dominant , we have ,

$$\overline{Y_F'^2} \propto \frac{\mu_t}{\bar{\rho}} \frac{k}{\varepsilon} \left(\frac{\partial \bar{Y}_F}{\partial y} \right)^2 \tag{2.16}$$

This assumption is particularly good in in the near - wall region This is the region of importance because most of the chemical reaction takes place near wall .

(2.d) Solid Propellant Burning Rate Equation

We express burning rate , r_b , of solid propellant by Arrhenius law of surface pyrolysis

$$r_b = A_s \exp\left(- \frac{E_{as}}{R_u T_{ps}} \right) \qquad (2\cdot17)$$

(2.e) Boundary Conditions

We need to specify the boundary conditions to solve the conservation equations at the solid - gas interface and freestream edge of the boundary layer.

(I) At the solid - gas interface / wall

(i) $\bar{u} = 0$ (2·18a)

(ii) $\bar{v} = \frac{\rho_s r_b}{\rho_w}$ (2·18b)

(iii) $\bar{T} = T_{ps}$ (2·18c)

(iv) The mass balance equation at the interface can be written as follows

total mass of the species k vapourised from the solid phase = mass of the species k transported away from the interface by the normal velocity in gas phase + mass of the species k transported from solid to gas by diffusion

Or,

$$(\bar{\rho}\, \bar{v}\, \bar{Y}_i)_w - \rho_s r_b Y_{is} - \left(\bar{\rho}\, D \frac{\partial \bar{Y}_i}{\partial y} \right)_w = 0 \qquad (2\cdot19)$$

where , $i \equiv F$ or O

(v) The energy balance is written as

$$\lambda_s \left. \frac{\partial T_p}{\partial y} \right|_w = \lambda \left. \frac{\partial \bar{T}}{\partial y} \right|_w + \rho_s r_b (h_{w-} - h_{w+}) \qquad (2\cdot20)$$

In Eq (2.22) , first term, on the left hand side represents the net heat flux to the solid propellant , the first term on the right hand side represents the heat flux from gas to solid surface and the second term represents the net heat release at the surface. Subscripts ' - ' and ' + ' are respectively for the solid and gas side of the interface

If we assume that heat conduction into the solid propellant is dominant in a direction normal to the burning surface , the heat conduction equation in the solid phase can be written as ,

$$\lambda_s \frac{\partial^2 T_p}{\partial y^2} = \rho_s C_s r_b \frac{\partial T_p}{\partial y} \quad \text{for} \quad -\infty < y \leq 0 \qquad (2\cdot21)$$

Integrating Eq (2.23) from $y = -\infty$, where $T_p = T_{pi}$ and $\lambda_s \frac{\partial T_p}{\partial y} = 0$ to $y = 0$, where $T_p = T_{ps}$, we get

$$\lambda_s \left. \frac{\partial T_p}{\partial y} \right|_w = \rho_s C_s r_b (T_{ps} - T_{pi}) \qquad (2\cdot22)$$

The net heat release at the surface per unit mass which is equal to the difference between the enthalpies of the gas and solid (on their respective sides of the interface) , can be expressed as (see Ref 8) :

$$Q_s (T_{ps}) = h_{w+} - h_{w-} = \bar{Q}_s + (C_p - C_s) (T_{ps} - \bar{T}_{ps}) \qquad (2\cdot23)$$

where , $\bar{Q}_s$ is the net surface heat release at a surface temperature , $\bar{T}_{ps}$.

Combining Eqs (2.22), (2.24) and (2.25) , we get

$$\left.\frac{\partial \bar{T}}{\partial y}\right|_N = \rho_f r_t \left[C_F T_{pS} - C_f T_{pf} + \bar{Q}_S + (C_f - C_F) \bar{T}_{pS} \right] \qquad (2\cdot24)$$

(vi) The boundary conditions for k and ε are to be applied near the wall and not at the wall because in the low Reynolds number zone in the vicinity of the wall , k - ε model is not valid (Ref.18 , p 684).

Near a wall , the production and dissipation terms in the k -equation are equated , assuming that only these terms dominant (a reasonable assumption at the edge of low Reynolds number turbulent region) . Thus ,

$$\varepsilon = \frac{\mu_t}{\bar{\rho}} \left(\frac{\partial \bar{u}}{\partial y} \right)^2 \qquad (2\cdot25)$$

The eddy viscosity , μ_t near the wall is calculated using a modification of Von Driest formula[15] ,

$$\mu_t = \bar{\rho} \left[K D_v (y + \Delta y) \right]^2 \left| \frac{\partial \bar{u}}{\partial y} \right| \qquad (2\cdot26)$$

The damping coefficient D_v , is altered to include the effect of surface roughness and the effect of local shear stress

$$D_v = 1 - \exp \left(- \frac{(y + \Delta y) \bar{\rho} u_* }{A^+ \mu} \frac{\tau}{\tau_w} \right) \qquad (2\cdot27)$$

where ,

$$\Delta y = 0.9 \frac{\mu}{\bar{\rho} u_*} \left[\sqrt{R_h^+} - R_h^+ \exp \left(- \frac{R_h^+}{6} \right) \right] \qquad (2\cdot28)$$

and ,

$$R_h^+ = \frac{\bar{\rho} u_* R_h}{\mu} \qquad (2\cdot29)$$

Eliminating μ_t from Eqs. (2.27) ; (2.28) and (2.11) , we get

$$k = \frac{\left[K D_v (y + \Delta y) \right]^2}{\sqrt{C_\mu}} \left(\frac{\partial \bar{u}}{\partial y} \right)^2 \qquad (2\cdot30)$$

$$\varepsilon = \left[K D_D (y + \Delta y) \right]^2 \left| \frac{\partial \bar{U}}{\partial y} \right|^3 \qquad (2.31)$$

(II) At the freestream

(i) $\bar{U} = U_\infty$ (2.32a)

(ii) $\bar{T} = T_\infty$ (2.32b)

(iii) $\bar{Y}_F = \bar{Y}_O = 0$ (2.32c)

(iv) $\frac{\partial k}{\partial y} = \frac{\partial \varepsilon}{\partial y} = 0$ (2.32d)

With the above set of boundary conditions at the wall and freestream , the mathematical formulation of the problem is complete. Next we have to solve the set of conservation equations subjected to the above-stated boundary conditions

Chapter 3 | Patankar - Spalding Transformation

The set of conservation equations (2.2 to 2.4 and 2.9 to 2.10) is a system of partial difference equations which is to be solved simultaneously.This system is parabolic in nature and involves non-linear terms.In this work , this system of equations is solved numerically by a very popular technique proposed by Patankar and Spalding [20] In this chapter, the conservation equations will be transformed to Patankar and Spalding cordinates.

(3.a) The Choice of Co-ordinate System

Fig.2 shows the boundary layer over a flat plate , and attached is a system of cartesian ($x \sim y$) coordinates.The drawback of this coordinate system is that it puts only few points in within the boundary layer where it is thin and so can't provide high accuracy there.Similar is the case with Von Mises coordinates ($x \sim \psi$) , shown in Fig.3.What is wanted is , if accuracy and computational economy are to be combined, is a grid which conforms better to the actual shape of the bopundary layer. For this , Patankar and Spalding have suggested a coordinate system in which cross-stream coordinate is represented by non-dimensional stream function , ω , defined as

$$\omega = \frac{\psi - \psi_I}{\psi_E - \psi_I} \qquad (3.1)$$

where ψ_I and ψ_E are functions of x alone.Fig.4 shows this system (x , ω) of coordinates called Patankar and Spalding co-ordinate system To transform the conservation equations in ($x \sim \omega$) coordinates , it is needed to transform them first in ($x \sim \psi$) coordinates which is done in the next section.

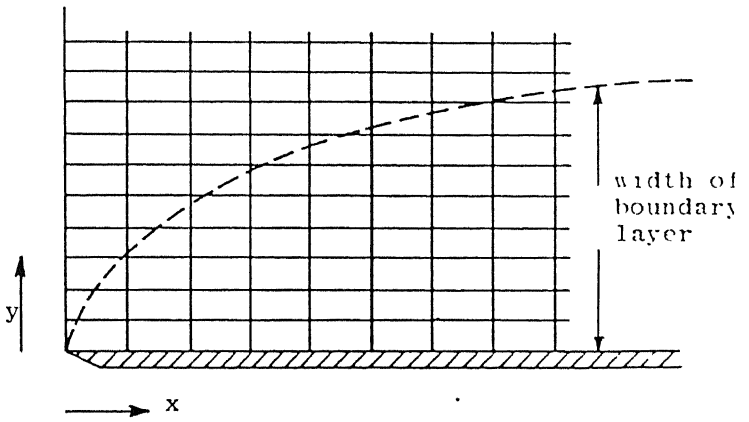

FIG 2 BOUNDARY LAYER OVER A FLAT PLATE WITH $x \sim$ COORDINATES

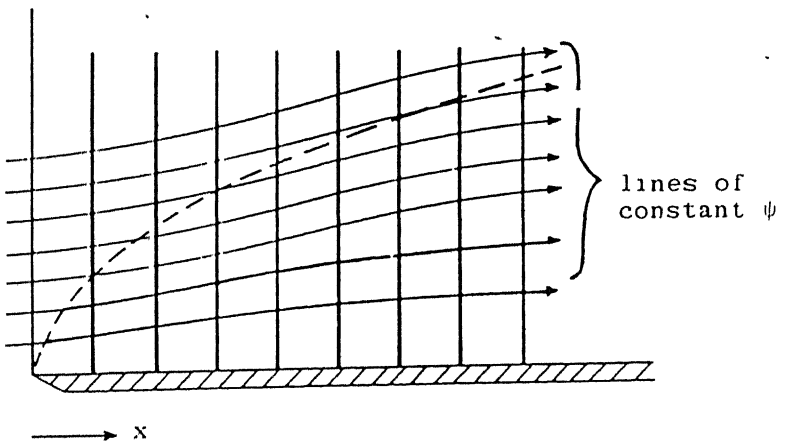

FIG.3 BOUNDARY LAYER OVER A FLAT PLATE WITH $x \sim \psi$ COORDINATES

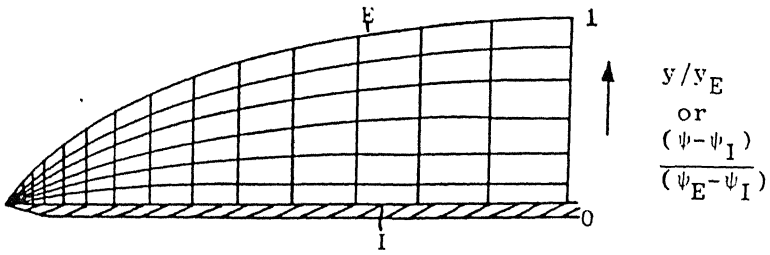

FIG.4 BOUNDARY LAYER OVER A FLAT PLATE WITH $x \sim \omega$ COORDINATES.

(3 b) Transformation to Von Mises Co-ordinates

The stream function ψ is defined by

$$\frac{\partial \psi}{\partial y} = \bar{\rho}\,\bar{u} \qquad (3\cdot2a)$$

and, $$\frac{\partial \psi}{\partial x} = -\,\bar{\rho}\,\bar{v} \qquad (3\cdot2b)$$

with

$$\frac{\partial \psi_I}{\partial x} = -\,\dot{m}_I \qquad (3\cdot3a)$$

$$\frac{\partial \psi_E}{\partial x} = -\,\dot{m}_E \qquad (3\cdot3b)$$

We have to transform ,say a function f in (x , y) coordinates to (x , ω) coordinates.From Calculus ,

$$\left(\frac{\partial f}{\partial x}\right)_y = \left(\frac{\partial f}{\partial x}\right)_\psi \left(\frac{\partial x}{\partial x}\right)_y + \left(\frac{\partial f}{\partial \psi}\right)_x \left(\frac{\partial \psi}{\partial x}\right)_y$$

Or,simply in operator form

$$\left(\frac{\partial}{\partial x}\right)_y = \left(\frac{\partial}{\partial x}\right)_\psi \left(\frac{\partial x}{\partial x}\right)_y + \left(\frac{\partial}{\partial \psi}\right)_x \left(\frac{\partial \psi}{\partial x}\right)_y \qquad (3\cdot4)$$

Since $\left(\frac{\partial x}{\partial x}\right)_y = 1$ and making use of Eq (3.2b) , we get

$$\left(\frac{\partial}{\partial x}\right)_y = \left(\frac{\partial}{\partial x}\right)_\psi - \bar{\rho}\,\bar{v}\left(\frac{\partial}{\partial \psi}\right)_x \qquad (3\cdot5)$$

Similarly , making use of Eq.(3.2a) , we get

$$\left(\frac{\partial}{\partial y}\right)_x = \bar{\rho}\,\bar{u}\left(\frac{\partial}{\partial \psi}\right)_x \qquad (3\cdot6)$$

With the help of transformation relations (3.5) and (3.6) , we can write the conservation equations (2.2 to 2.4 and 2.9 to 2.10) in the following general form (dropping the subscripts in Eqs. (3.5) and (3.6) , assuming that their

meaning is understood)

$$\frac{\partial \phi}{\partial x} = \frac{\partial}{\partial \psi}\left(\bar{\rho}\, \bar{u}\, \Gamma_{\phi,eff} \frac{\partial \phi}{\partial \psi} \right) + \frac{1}{\bar{\rho}\, \bar{u}} S_{\phi} \qquad (3.7)$$

where ϕ stands for any of the flow variables , S_{ϕ} is the source term corresponding to the variable and $\Gamma_{\phi,eff}$ is the effective value of the transport property in the flux law of ϕ. In Table 1 , $\Gamma_{\phi,eff}$ and S_{ϕ} for all the conservation equations are shown.

Table 1 : Conservation Equations in (x ~ ψ) Co-ordinates

Eq No	ϕ	$\Gamma_{\phi,eff}$	S_{ϕ}
(2.2)	$\bar{u}$	μ_{eff}	$-\frac{d\bar{p}}{dx}$
(2.3a)	$\bar{Y}_F$	$\left(\frac{\mu}{Sc}\right)_{eff}$	$\bar{\dot{\omega}}_F$
(2.3c)	$\bar{Y}_{OF}$	$\left(\frac{\mu}{Sc}\right)_{eff}$	0
(2.4)	$\bar{H}$	$\left(\frac{\mu}{Pr}\right)_{eff}$	$\frac{\partial}{\partial y}\left\{ \left[\mu_{eff} - \left(\frac{\mu}{Pr}\right)_{eff} \right] \frac{\partial \frac{\bar{u}^2}{2}}{\partial y} \right\}$
(2.9)	k	$\mu + \frac{\mu_t}{C_1}$	$\mu_t \left(\frac{\partial \bar{u}}{\partial y}\right)^2 - \bar{\rho}\, \varepsilon$
(2.10)	ε	$\mu + \frac{\mu_t}{C_2}$	$C_3\, \mu_t \left(\frac{\partial \bar{u}}{\partial y}\right)^2 \frac{\varepsilon}{k} - C_4\, \bar{\rho}\, \frac{\varepsilon^2}{k}$

(3.c) Transformation to Patankar - Spalding Co-ordinate System

Here , the problem is to transform a function f (x , ψ) to f (x , ω). We can write equations (in the operator form) similar to Eq.(3.4)

$$\left(\frac{\partial}{\partial x} \right)_{\psi} = \left(\frac{\partial}{\partial x} \right)_{\omega} \left(\frac{\partial x}{\partial x} \right)_{\psi} + \left(\frac{\partial}{\partial \omega} \right)_{x} \left(\frac{\partial \omega}{\partial x} \right)_{\psi}$$

$$\left(\frac{\partial}{\partial \psi} \right)_{x} = \left(\frac{\partial}{\partial x} \right)_{\omega} \left(\frac{\partial x}{\partial \omega} \right)_{\psi} + \left(\frac{\partial}{\partial \omega} \right)_{x} \left(\frac{\partial \omega}{\partial \psi} \right)_{x}$$

Since , $\left(\frac{\partial x}{\partial x} \right)_{\omega} = 1$ and $\left(\frac{\partial x}{\partial \omega} \right)_{\psi} = 0$

the above equations reduce to

$$\left(\frac{\partial}{\partial x} \right)_{\psi} = \left(\frac{\partial}{\partial x} \right)_{\omega} + \left(\frac{\partial}{\partial \omega} \right)_{x} \left(\frac{\partial \omega}{\partial x} \right)_{\psi} \qquad (3.8)$$

and $$\left(\frac{\partial}{\partial \psi} \right)_{x} = \left(\frac{\partial}{\partial \omega} \right)_{x} \left(\frac{\partial \omega}{\partial \psi} \right)_{x} \qquad (3.9)$$

To evaluate $\left[\frac{\partial \omega}{\partial x} \right]_{\psi}$ and $\left[\frac{\partial \omega}{\partial \psi} \right]_{x}$, we write Eq.(3.1) as

$$\psi = \psi_{I} + \omega \left(\psi_{E} - \psi_{I} \right) \qquad (3.10)$$

remembering that ψ_{I} and ψ_{E} are functions of x alone .

From calculus , total change in ψ as a function of x and ω can be written as

$$d\psi = \left(\frac{\partial \psi}{\partial x} \right)_{\omega} dx + \left(\frac{\partial \psi}{\partial \omega} \right)_{x} d\omega \qquad (3.11)$$

If ψ is constant , then $d\psi = 0$. Therefore , from Eq.(3.11)

$$\left(\frac{\partial \omega}{\partial x} \right)_{\psi} = - \frac{\left(\frac{\partial \psi}{\partial x} \right)_{\omega}}{\left(\frac{\partial \psi}{\partial \omega} \right)_{x}} \qquad (3.12)$$

From Eq (3.10) ,

$$\left(\frac{\partial \psi}{\partial x} \right)_{\omega} = \frac{d\psi_I}{dx} + \omega \frac{d}{dx} \left(\psi_E - \psi_I \right) \tag{3·13}$$

and,

$$\left(\frac{\partial \psi}{\partial \omega} \right)_x = \left(\psi_E - \psi_I \right) \tag{3·14}$$

Using Eqs (3.13) and (3.14) , Eq (3.12) can be expressed as

$$\left(\frac{\partial \omega}{\partial x} \right)_{\psi} = - \frac{1}{\left(\psi_E - \psi_I \right)} \left[\frac{d\psi_I}{dx} + \omega \frac{d}{dx} \left(\psi_E - \psi_I \right) \right] \tag{3·15}$$

Further, from Eqs (3.11) and (3.14) , we obtain

$$\left(\frac{\partial \omega}{\partial \psi} \right)_x = \frac{1}{\left(\frac{\partial \psi}{\partial \omega} \right)_x} = \frac{1}{\left(\psi_E - \psi_I \right)} \tag{3·16}$$

Making use of these results in Eqs. (3.8) and (3.9) , we get

$$\left(\frac{\partial}{\partial x} \right)_{\psi} = \left(\frac{\partial}{\partial x} \right)_{\omega} + \left(a + b\, \omega \right) \left(\frac{\partial}{\partial \omega} \right)_x \tag{3·17}$$

$$\left(\frac{\partial}{\partial \psi} \right)_x = \frac{1}{\left(\psi_E - \psi_I \right)} \left(\frac{\partial}{\partial \omega} \right)_x \tag{3·18}$$

where,

$$a \equiv - \frac{1}{\left(\psi_E - \psi_I \right)} \frac{d\psi_I}{dx} \tag{3·19}$$

$$b \equiv - \frac{1}{\left(\psi_E - \psi_I \right)} \frac{d}{dx} \left(\psi_E - \psi_I \right) \tag{3·20}$$

With the help of the transformation relations (3.16) and (3.17) , the general form of the conservation equations , Eq.(3.7) , can be written in the following form

$$\frac{\partial \phi}{\partial x} + \left(a + b\, \omega \right) \frac{\partial \phi}{\partial \omega} = \frac{\partial}{\partial \omega} \left[\frac{\bar{\rho}\, \bar{u}\, \Gamma_{\phi,eff}}{\left(\psi_E - \psi_I \right)^2} \frac{\partial \phi}{\partial \omega} \right] + \frac{1}{\bar{\rho}\, \bar{u}} S_{\phi}$$

Or,

$$\frac{\partial \phi}{\partial x} + \left(a + b\, \omega \right) \frac{\partial \phi}{\partial \omega} = \frac{\partial}{\partial \omega} \left(c \frac{\partial \phi}{\partial \omega} \right) + d \tag{3·21}$$

with

$$c = \frac{\bar{\rho}\,\bar{u}\,\Gamma_{\phi,eff}}{(\psi_E - \psi_I)^2} \tag{3.22}$$

$$d = \frac{1}{\bar{\rho}\,\bar{u}}\,S_\phi \tag{3.23}$$

In Table 2 , c and d for all the conservation equations are presented

Eq.(3.20) is the general form of conservation equations. Some remarkable features of this equation are :

(i) In view of Eqs (3.3a) and (3.3b) , we have from Eqs. (3.18) and (3.19)

$$a \equiv \frac{\dot{m}_I}{(\psi_E - \psi_I)} \tag{3.24}$$

$$b \equiv \frac{\dot{m}_E - \dot{m}_I}{(\psi_E - \psi_I)} \tag{3.25}$$

where the mass fluxes $\dot{m}_E$ are $\dot{m}_I$ are the mass flow rates per unit area divided by (ψ_E - ψ_I) across the grid boundaries, and are positive for flow in positive y-direction.Thus , (a + b ω) denotes the mass flow rate across the line of constant ω , divided by (ψ_E - ψ_I).

(ii) Patankar - Spalding coordinate system has an extra advantage over the choice of (y/y_E) as a variable (if chosen , instead of ω). For a constant x , (a + b ω) is a function of ω alone , but with (y/y_E) as avariable , this coefficient would have involved an integral over that variable of the forward velocity , thereby , making this coefficient more troublesome to evaluate.

Table 2 Conservation Equations in (x ~ ω) Coordinates

Eq No	ϕ	c	d
(2·2)	$\bar{u}$	$\dfrac{\bar{\rho}\,\bar{u}\,\mu_{eff}}{(\psi_E - \psi_I)^2}$	$-\dfrac{1}{\bar{\rho}\bar{u}}\dfrac{d\bar{p}}{dx}$
(2·3a)	$\bar{Y}_F$	$\dfrac{\bar{\rho}\,\bar{u}}{(\psi_E - \psi_I)^2}\left(\dfrac{\mu}{Sc}\right)_{eff}$	$\dfrac{1}{\bar{\rho}\bar{u}}\bar{\omega}_F$
(2·3c)	$\bar{Y}_{OF}$	$\dfrac{\bar{\rho}\,\bar{u}}{(\psi_E - \psi_I)^2}\left(\dfrac{\mu}{Sc}\right)_{eff}$	0
(2·4)	$\bar{H}$	$\dfrac{\bar{\rho}\,\bar{u}}{(\psi_E - \psi_I)^2}\left(\dfrac{\mu}{Pr}\right)_{eff}$	$\dfrac{1}{\bar{\rho}\bar{u}}\dfrac{\partial}{\partial y}\left\{\left[\mu_{eff} - \left(\dfrac{\mu}{Pr}\right)_{eff}\right]\dfrac{\partial \bar{u}^2/2}{\partial y}\right\}$
(2·9)	k	$\dfrac{\bar{\rho}\,\bar{u}}{(\psi_E - \psi_I)^2}\left[\mu + \dfrac{\mu_t}{C_1}\right]$	$\dfrac{1}{\bar{\rho}\bar{u}}\left[\mu_t\left(\dfrac{\partial \bar{u}}{\partial y}\right)^2 - \bar{\rho}\,\epsilon\right]$
(2·10)	ϵ	$\dfrac{\bar{\rho}\,\bar{u}}{(\psi_E - \psi_I)^2}\left[\mu + \dfrac{\mu_t}{C_2}\right]$	$\dfrac{1}{\bar{\rho}\bar{u}}\left[C_3\,\mu_t\left(\dfrac{\partial \bar{u}}{\partial y}\right)^2\dfrac{\epsilon}{k} - C_4\,\bar{\rho}\,\dfrac{\epsilon^2}{k}\right]$

Chapter 4 | Method Of Solution

As we have seen in the previous chapter , all the conservation eqations can be represented by the general form , Eq (3.20).To solve this type of equation which is parabolic in nature , we use the methodology due to Patankar and Spalding This is a marching technique , that is , the finite difference eqations are solved at the succesive x-stations, using the solutions at the previous x-location. In this chapter , first transformed conservation equations (Table 2) are cast into a set of finite difference equations and then some salient features of the solution procedure will be described in brief.

(4.a) Finite Differencing of Equations

In Patankar and Spalding method , implicit finite differencing is done which connects the value of a dependent variable , $\phi_{i,D}$, at a downstream location node i , with the values at the two neighbouring nodes at the same x-location , $\phi_{i-1,D}$ and $\phi_{i+1,D}$ and with the values at the three corresponding upstream nodes , $\phi_{i-1,U}$, $\phi_{i,U}$ and $\phi_{i+1,U}$. Equivalently, it can be written in the following form .

$$D_i \phi_{i,D} = A_i \phi_{i+1,D} + B_i \phi_{i-1,D} + C_i \qquad (4.1)$$

where A_i , B_i , C_i and D_i are coefficients for which expressions are to be derived by integrating Eq.(3.20) over an appropriate control volume (see Fig.6) It should be noted that the coefficient C_i carries the effect of the upstream (i.e. previous x-location) node(s).

Before we start integration over the control volume , it is

necessary to employ a ϕ-profile assumption We show this assumed profile in Fig 5 Halfway between adjacent pairs of grid points in the range 2 to (N-1) are drawn vertical broken lines , dividing the whole ω-range into (N-1) intervals The value of any variable ϕ is supposed to be uniform within the interval.

The control volumes , over which we are going to integrate Eq (3 20),are illustrated in Fig 6 The boundaries of all the control volumes except the two near the edges are represented by

upper edge : $\omega_{i+\frac{1}{2}} = \frac{1}{2} (\omega_{i+1} + \omega_i)$ (4 2)

lower edge : $\omega_{i-\frac{1}{2}} = \frac{1}{2} (\omega_i + \omega_{i-1})$ (4 3)

The lower edges of the control volume near I boundary (i.e for i equal to 2) is

$$\omega_{i-\frac{1}{2}} = 0 \qquad (4\ 4)$$

Also,the upper edge of the control volume near the E boundary (i e for i equal to N -1) is

$$\omega_{i+\frac{1}{2}} = 1 \qquad (4.5)$$

We will satisfy conservation equations for each of the control volumes and thus conservation will be satisfied for the whole boundary layer.Integrating Eq (3.20) over i^{th} control volume , we get

$$\frac{1}{\delta x} \int_{i-\frac{1}{2}}^{i+\frac{1}{2}} (\phi_D - \phi_U)\, d\omega \qquad \text{term (i)}$$

$$+ \left\{ (a + b\omega)\, \phi \right\}_{i-\frac{1}{2},M}^{i+\frac{1}{2},M} \qquad \text{term (ii)}$$

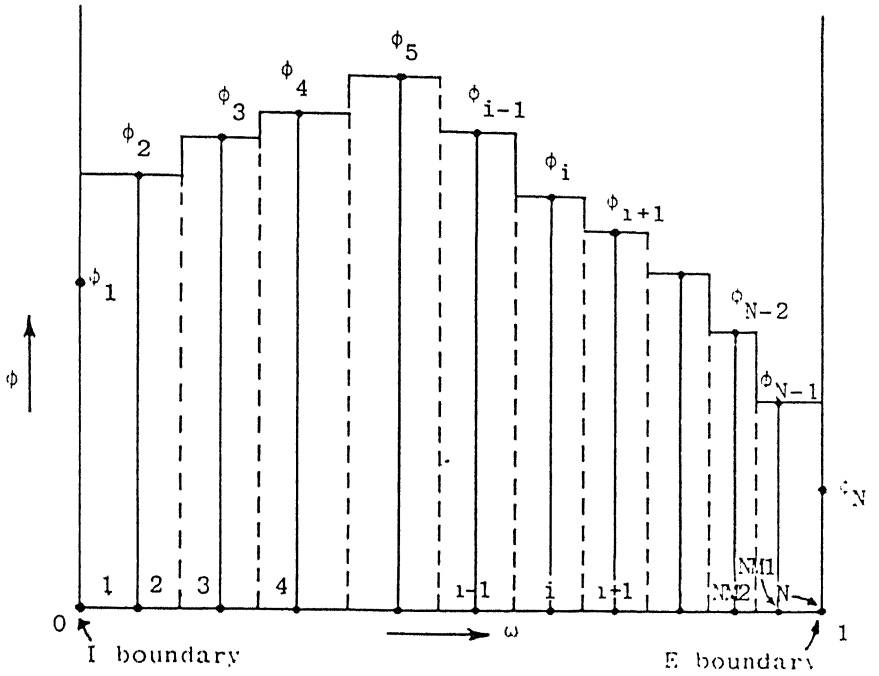

FIG.5 ϕ - PROFILE ASSUMPTION FOR FINITE DIFFERENCING

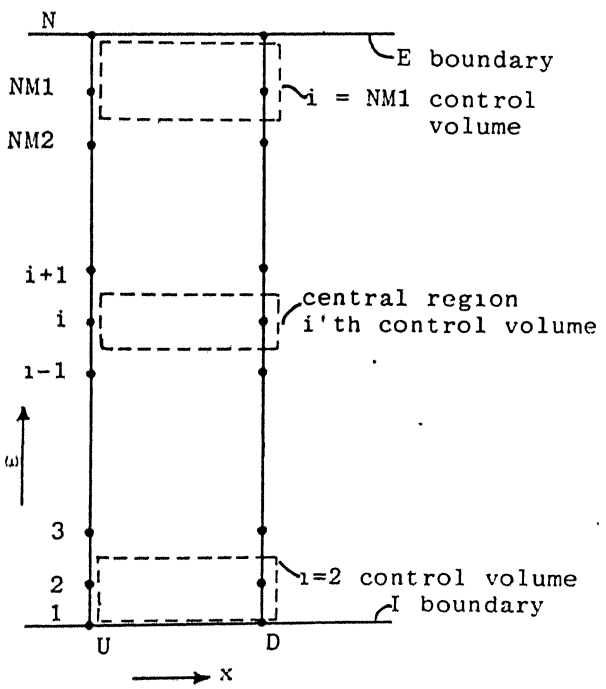

FIG.6 THE CONTROL VOLUMES USED FOR THE DERIVATION OF THE FINITE DIFFERENCE EQUATIONS

$$-\left[\left[b\left[\int_{1-\frac{1}{2}}^{1+\frac{1}{2}}\phi\ d\omega\right]\right]\right]_M \qquad \text{term (iii)}$$

$$=\left[c\ \frac{\partial\phi}{\partial\omega}\right]_{i-\frac{1}{2},M}^{i+\frac{1}{2},M} \qquad \text{term (iv)}$$

$$+\left[\int_{i-\frac{1}{2}}^{i+\frac{1}{2}} d\ d\omega\right]_M \qquad \text{term (v)} \qquad (4.6)$$

Where subscripts U , D and M stands for upstream , downstream and intermediate x-location.With the ϕ-profile assumption of Fig 5 , various terms of Eq.(4.6) can be written as follows

(i) : $$\frac{(\phi_{i,D}-\phi_{i,U})}{\delta x}\left(\omega_{i+\frac{1}{2}}-\omega_{i-\frac{1}{2}}\right) \qquad (4.7)$$

(iii) : $$-b_{x=M}\ \phi_{i,M}\ \left(\omega_{i+\frac{1}{2}}-\omega_{i-\frac{1}{2}}\right) \qquad (4.8)$$

$$\text{with}\quad b_{x=M}=-\frac{1}{(\psi_E-\psi_I)_U}\ \frac{(\psi_E-\psi_I)_D-(\psi_E-\psi_I)_U}{\delta x}$$

And choosing $\phi_{i,M}=\phi_{i,D}$, first and third term can be added to represent the x-direction convection of ϕ : -

(i) + (iii)

$$\left[\frac{(\psi_E - \psi_I)_D}{(\psi_E - \psi_I)_U} \phi_{i,D} - \phi_{i,U} \right] \frac{\left[\omega_{i+\frac{1}{2}} - \omega_{i-\frac{1}{2}} \right]}{\delta x} \qquad (4.9)$$

In view of Eq (3.23) and Eq (3.24)

$$(a + b \omega) \equiv \frac{1}{(\psi_E - \psi_I)_U} \left[\dot{m}_I + \omega (\dot{m}_E - \dot{m}_I) \right] \qquad (4.10)$$

so that

$$a + b \omega|_{i+\frac{1}{2}} = \frac{\dot{m}_{i+\frac{1}{2}}}{(\psi_E - \psi_I)_U} \qquad (4.11)$$

where , $\dot{m}_{i+\frac{1}{2}} = \dot{m}_I + \omega_{i+\frac{1}{2}} (\dot{m}_E - \dot{m}_I)$ (4.12)

Similarly , $a + b \omega|_{i-\frac{1}{2}} = \frac{\dot{m}_{i-\frac{1}{2}}}{(\psi_E - \psi_I)_U}$ (4.13)

with , $\dot{m}_{i-\frac{1}{2}} = \dot{m}_I + \omega_{i-\frac{1}{2}} (\dot{m}_E - \dot{m}_I)$ (4.14)

Therefore second term can be written as

$$\textbf{(ii)} : \quad \frac{1}{(\psi_E - \psi_I)_U} \left[\dot{m}_{i+\frac{1}{2}} \phi_{i+\frac{1}{2}} - \dot{m}_{i-\frac{1}{2}} \phi_{i-\frac{1}{2}} \right]_M \qquad (4.15)$$

Choosing M as the downstream location , that is , $\phi_{i,M} \equiv \phi_{i,D}$

and , $\phi_{i+\frac{1}{2}} = (\phi_{i+1} + \phi_i)$ (4.16a)

$\phi_{i-\frac{1}{2}} = (\phi_{i-1} + \phi_i)$ (4.16b)

With these , (4.15) can be written as

$$\textbf{(ii)} : \quad \frac{1}{2(\psi_E - \psi_I)_U} \left[\dot{m}_{i+\frac{1}{2}} \phi_{i+1} + (\dot{m}_{i+\frac{1}{2}} - \dot{m}_{i-\frac{1}{2}}) \phi_i - \dot{m}_{i-\frac{1}{2}} \phi_{i-1} \right]_M \qquad (4.17)$$

The diffusive term (iv) can be rewritten as follows

$$\left[C \frac{\partial \phi}{\partial \omega} \right]_{i+\frac{1}{2},M} = \frac{1}{(\psi_E - \psi_I)_U} \left[\Gamma_{\phi,eff} \frac{\partial \phi}{\partial y} \right]_{i+\frac{1}{2},M} \quad (4\ 18)$$

and ,

$$\left[C \frac{\partial \phi}{\partial \omega} \right]_{i-\frac{1}{2},M} = \frac{1}{(\psi_E - \psi_I)_U} \left[\Gamma_{\phi,eff} \frac{\partial \phi}{\partial y} \right]_{i-\frac{1}{2},M} \quad (4.19)$$

If it is assumed that ,

$$\left[\frac{\partial \phi}{\partial y} \right]_{i+\frac{1}{2},M} = \frac{(\phi_{i+1} - \phi_i)_D}{(y_{i+1} - y_i)_U} \quad (4\ 20a)$$

$$\left[\frac{\partial \phi}{\partial y} \right]_{i-\frac{1}{2},M} = \frac{(\phi_i - \phi_{i-1})_D}{(y_i - y_{i-1})_U} \quad (4\ 20b)$$

term (iv) can be written as

$$\textbf{(iv)} : \quad \frac{1}{(\psi_E - \psi_I)_U} \left[T_{i+\frac{1}{2}} (\phi_{i+1} - \phi_i)_D - T_{i-\frac{1}{2}} (\phi_i - \phi_{i-1})_D \right] \quad (4\ 21)$$

$$\text{where,} \quad T_{i+\frac{1}{2}} = \frac{\Gamma_{\phi,eff} \big|_{i+\frac{1}{2}}}{(y_{i+1} - y_i)_U} \quad (4\ 22)$$

$$\text{and ,} \quad T_{i-\frac{1}{2}} = \frac{\Gamma_{\phi,eff} \big|_{i-\frac{1}{2}}}{(y_i - y_{i-1})_U} \quad (4.23)$$

The source term (v).represents the effect of sources of ϕ within the control volume per unit increment of x Although sources are non-linear functions of ϕ in general , these terms are evaluated by adding in upstream values a term

depending linearly on ϕ

$$(v): \quad \int_{i-\frac{1}{2}}^{i+\frac{1}{2}} d_{i,D}\, d\omega = S_i + S_i' \phi_{i,D} \tag{4.24}$$

In the next section, source linearization procedure will be presented, that is, the expressions for S_i and S_i' for each individual conservation equation will be derived

Now, with the help of (4.9), (4.17), (4.21) and (4.23), Eq.(4.6) can be written in the following form.

$$\left\{ \frac{(\psi_E - \psi_I)_D}{(\psi_E - \psi_I)_U} \frac{(\omega_{i+\frac{1}{2}} - \omega_{i-\frac{1}{2}})}{\delta x} + \frac{1}{2(\psi_E - \psi_I)_U}(\dot{m}_{i+\frac{1}{2}} - \dot{m}_{i-\frac{1}{2}}) \right.$$

$$\left. + \frac{1}{(\psi_E - \psi_I)_U}(T_{i+\frac{1}{2}} - T_{i-\frac{1}{2}}) - S_i' \right\} \phi_{i,D}$$

$$= \left\{ \frac{1}{(\psi_E - \psi_I)_U}(T_{i+\frac{1}{2}} - \dot{m}_{i+\frac{1}{2}}) \right\} \phi_{i+1,D} + \left\{ \frac{1}{(\psi_E - \psi_I)_U}(T_{i-\frac{1}{2}} + \dot{m}_{i-\frac{1}{2}}) \right\} \phi_{i-1,D}$$

$$+ \left\{ \frac{(\omega_{i+\frac{1}{2}} - \omega_{i-\frac{1}{2}})}{\delta x} \phi_{i,U} + S_i \right\} \tag{4.25}$$

The first two terms in the coefficient of $\phi_{i,D}$ can be simplified with the help of Eqs (3.18),(3.19),(3.23) and (3.24) in the following way

we have, $$\frac{(\psi_E - \psi_I)_D}{(\psi_E - \psi_I)_U} = \left[1 - \frac{(\dot{m}_E - \dot{m}_I)}{(\psi_E - \psi_I)_U} \delta x \right]$$

therefore, $\dfrac{(\psi_E - \psi_I)_D}{(\psi_E - \psi_I)_U} \dfrac{(\omega_{i+\frac{1}{2}} - \omega_{i-\frac{1}{2}})}{\delta x}$

$$= \frac{(\omega_{i+\frac{1}{2}} - \omega_{i-\frac{1}{2}})}{\delta x} - \frac{1}{2(\psi_E - \psi_I)_U}(\dot{m}_{i+\frac{1}{2}} - \dot{m}_{i-\frac{1}{2}}) \qquad (4.26)$$

With the help of Eq (4.26), Eq (4.25) can be written as (after multiplying both sides by δx)

$$\left\{ (\omega_{i+\frac{1}{2}} - \omega_{i-\frac{1}{2}}) + \frac{\delta x}{(\psi_E - \psi_I)_U}(T_{i+\frac{1}{2}} - \dot{m}_{i+\frac{1}{2}}) + \frac{\delta x}{(\psi_E - \psi_I)_U}(T_{i-\frac{1}{2}} + \dot{m}_{i-\frac{1}{2}}) - S_i'\delta x \right\} \phi_{i,D}$$

$$= \left\{ \frac{\delta x}{(\psi_E - \psi_I)_U}(T_{i+\frac{1}{2}} - \dot{m}_{i+\frac{1}{2}}) \right\} \phi_{i+1,D} + \left\{ \frac{\delta x}{(\psi_E - \psi_I)_U}(T_{i-\frac{1}{2}} + \dot{m}_{i-\frac{1}{2}}) \right\} \phi_{i-1,D}$$

$$+ \left\{ (\omega_{i+\frac{1}{2}} - \omega_{i-\frac{1}{2}}) \phi_{i,U} + S_i \delta x \right\} \qquad (4.27)$$

Comparing Eq (4.27) with Eq (4.1), expressions for the coefficients A_i, B_i, C_i and D_i are obtained

$$A_i = \frac{\delta x}{(\psi_E - \psi_I)_U}(T_{i+\frac{1}{2}} - \dot{m}_{i+\frac{1}{2}}) \qquad (4.28)$$

$$B_i = \frac{\delta x}{(\psi_E - \psi_I)_U}(T_{i-\frac{1}{2}} + \dot{m}_{i-\frac{1}{2}}) \qquad (4.29)$$

$$C_i = (\omega_{i+\frac{1}{2}} - \omega_{i-\frac{1}{2}}) \phi_{i,U} + S_i \delta x \qquad (4.30)$$

$$D_i = (\omega_{i+\frac{1}{2}} - \omega_{i-\frac{1}{2}}) + A_i + B_i - S_i'\delta x \qquad (4.31)$$

The coefficients A_i and B_i are to be modified as these may become negative for high lateral mass flow rates and thus, may yield physically implausible values of $\phi_{i,D}$. The following modification is incorporated in this work (

see Ref 21 for details).

$$A_i = max\left[0 , \left\{ \frac{\delta x}{(\psi_E - \psi_I)_U} \left(T_{i+\frac{1}{2}} - \dot{m}_{i+\frac{1}{2}} \right) \right\} , - \left\{ \frac{\delta x}{(\psi_E - \psi_I)_U} \dot{m}_{i+\frac{1}{2}} \right\} \right] \quad (4.32)$$

$$E_{i+1} = max\left[0 , \left\{ \frac{\delta x}{(\psi_E - \psi_I)_U} \left(T_{i+\frac{1}{2}} + \dot{m}_{i+\frac{1}{2}} \right) \right\} \right] \quad (4.33)$$

Also transfer coefficients T 's are to be modified at the boundaries because

(i) at E-boundary , the grid adjoins the undisturbed flow and ϕ-gradients are zero

(ii) at I-boundary , due to the presence of a wall,there are sharp variations in transport properties. Also, special effects such as kinetic heating or chemical reaction , make the diffusive flux proportional not to ($\phi_1 - \phi_2$) but to some other difference

So,for i = 2 , $$T_{i-\frac{1}{2}} = \frac{J_\phi|_I}{(\phi_1 - \phi_2 - \delta\phi_I)} \quad (4.34)$$

and , for i = N-1 , $$T_{i+\frac{1}{2}} = 0 \quad (4.35)$$

where $J_\phi|_I$ stands for the diffusive flux of ϕ at the I boundary and $\delta\phi_I$ represents the above stated wall effects.For the E-boundary , $\delta\phi_E$ is zero.

(4 b) Source Linearization

The source term $d_{i,D}$ can be expanded by Taylor series (upto second term only as it is assumed that source of ϕ depends linearly on ϕ) in the following way

$$d_{i,D} = d_{i,U} + \left[\frac{\partial d}{\partial \phi} \right]_{i,U} (\phi_{i,D} - \phi_{i,U}) \quad (4.36)$$

Then we can obtain the following expressions for the coefficients S_i and S_i'

$$S_i = \left[d_{i,U} + \left[\frac{\partial d}{\partial \phi} \right]_{i,U} \phi_{i,U} \right] \left(\omega_{i+\frac{1}{2}} - \omega_{i-\frac{1}{2}} \right) \qquad (4.37)$$

$$S_i' = \left[\frac{\partial d}{\partial \phi} \right]_{i,U} \left(\omega_{i+\frac{1}{2}} - \omega_{i-\frac{1}{2}} \right) \qquad (4.38)$$

In Table 3, S_i and S_i' are presented for various conservation equations.

Table 3

Equation	S_i	S_i'
X-Mom	$\left[-\frac{2}{(\bar{\rho}\ \bar{u})_i} \frac{d\bar{p}}{dx} \right]_U \omega_{dif}$	$\left[\frac{2}{(\bar{\rho}\ \bar{u}^2)_i} \frac{d\bar{p}}{dx} \right]_U \omega_{dif}$
Energy	$\frac{1}{2(\psi_E - \psi_i)} F$	0
k-eq	$\left[\mu_t \left[\frac{\partial \bar{u}}{\partial y} \right]^2 + \frac{\varepsilon}{\bar{u}} \right]_{i,U} \omega_{dif}$	$-2\left[\frac{\varepsilon}{k\ \bar{u}} \right]_{i,U} \omega_{dif}$
ε-eq	$\left[\frac{C_4 \varepsilon^2}{k \bar{u}} \right]_{i,U} \omega_{dif}$	$\left[\frac{C_4\ \mu_t}{k} \left[\frac{\partial \bar{u}}{\partial y} \right]^2 - \frac{2 C_4 \varepsilon}{\bar{u}\ k} \right]_{i,U} \omega_{dif}$

where , $F = \left[T_{i+\frac{1}{2}} (\bar{u}_{i+1}^2 - \bar{u}_i^2) - T_{i-\frac{1}{2}} (\bar{u}_i^2 - \bar{u}_{i-1}^2) \right]_U$

and , $\omega_{dif} = \left(\omega_{i+\frac{1}{2}} - \omega_{i-\frac{1}{2}} \right)$

For fuel species conservation equation , source linearisation is done in the following way

$$d = -\frac{C_\omega \sqrt{k}}{\bar{u}} \left| \frac{\partial \bar{Y}_F}{\partial y} \right| = -\frac{C_\omega \sqrt{k\ \bar{\rho}\ \bar{u}}}{\bar{u}} \frac{1}{(\psi_E - \psi_i)} \left| \frac{\partial \bar{Y}_F}{\partial \omega} \right|$$

$$\text{or} \quad d = \frac{C_\omega \sqrt{k}\,\bar{\rho}}{(\psi_E - \psi_I)} \frac{\partial \bar{T}_F}{\partial U}$$

$$\text{therefore} \int_{-\frac{1}{2}}^{+\frac{1}{2}} d_D \, d\omega = \frac{C_\omega (\sqrt{k}\,\bar{\rho})_{i,0}}{2(\psi_E - \psi_I)_0} \left[(Y_F)_{i+1,0} - (Y_F)_{i-1,0} \right]$$

and subsequently the coefficients A_i and B_i are modified for this equation.

(4.c) Solution Procedure

The finite difference equation (4.27) gives rise a system of algebraic equations which are tri-diagonal in nature. These are solved by the tri-diagonal matrix algorithm (TDMA) described in Ref. 21. Around eighty grid points were considered and half of them were distributed with in 10% of the boundary layer thickness, where the flow variables have sharp gradients. The forward step-size is calculated in two ways: (i) based on boundary layer thickness (equal to 0.3 times the boundary layer thickness) (ii) based on the mass flow rate at I & E boundaries (Ref.20) . In the program the actual step size was taken to be minimum of the two. The initial wall values of temperature, fuel and oxidation mass fractions were guessed and then iterations were performed until the boundary conditions at the wall are satisfied

In Appendix-C, the flow chart and descriptions of various subroutines is presented.

Chapter 5 | Results,Discussions And Conclusions

(5 a) Results and Discussions

Numerical computations were done for two types of composite propellant compositions (1) Ammonium perchlorate (75%) and PBAA/EPON (25%) and (2) Ammonium perchlorate (65%) and Polysulphide (35%) The basic aim behind these calculations is to predict the effect of freestream velocity on the burning rate under typical flow conditions, similar to those prevailing in an actual rocket motor This was done by varying the freestream velocity in a reasonable range The various physical properties which were used in calculations alongwith the constants used in turbulence modeling are listed in Appendix B The details of the procedures followed in obtaining some of the properties are described in Ref 8 While calculating the parameters associated with the global single-step-forward reaction,it is assumed that primary flame collapses at the propellant surface,merely depositing its heat there as the gasification takes place(see Ref 2)

Non-dimensional velocity (u/U_∞) and temperature $(T-T_{ps})/(T_\infty-T_{ps})$ profiles are shown in Fig.7 and Fig.8. The velocity gradient is maximum at the propellant surface and decreases monotonically to nearly zero value at the freestream edge. The temperature rises rapidly in the near-wall region from its value at the propellant surface and then gradually approaches the freestream value The rapid rise in the near-wall region is brought about by the chemical

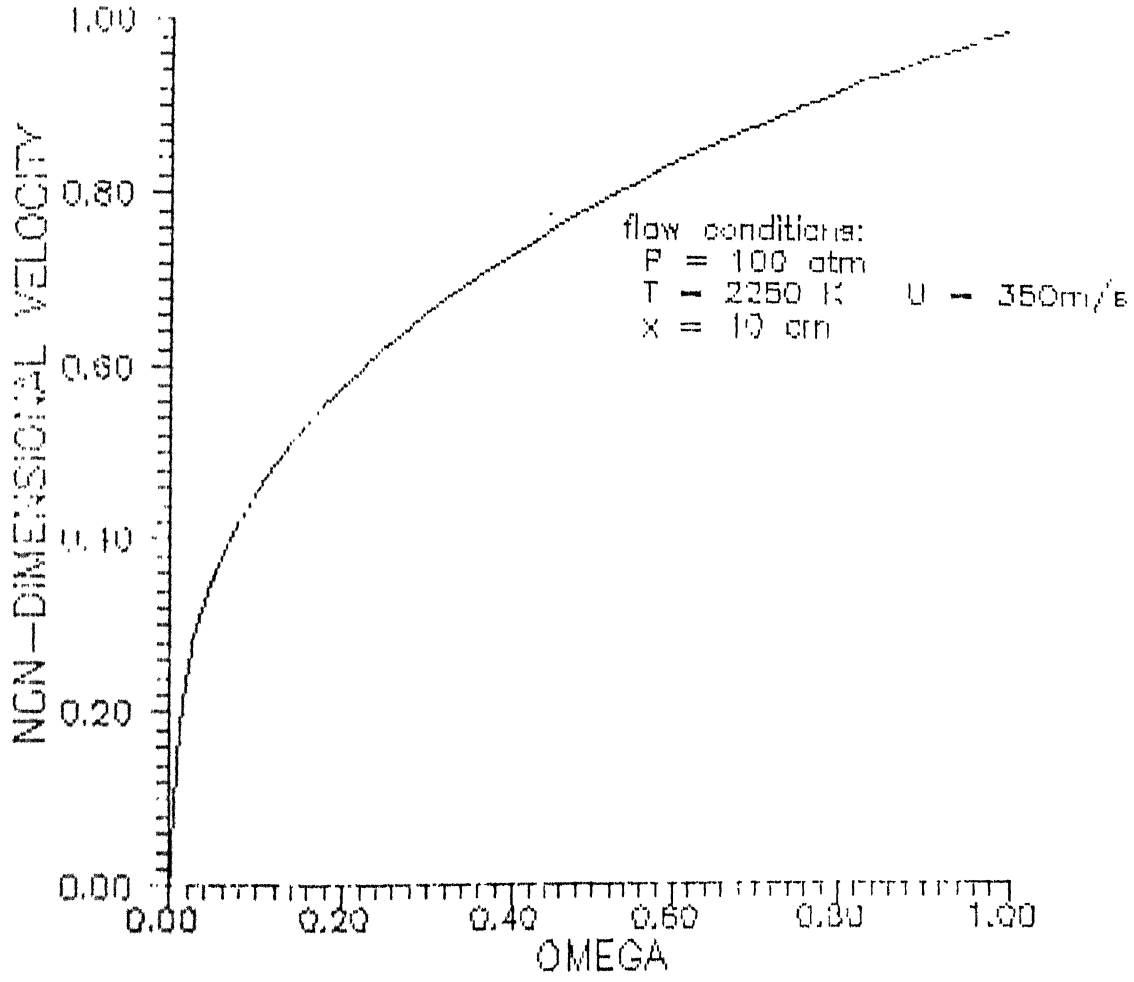

FIG.7 NON - DIMENSIONAL VELOCITY (u/U$_\infty$) PROFILE

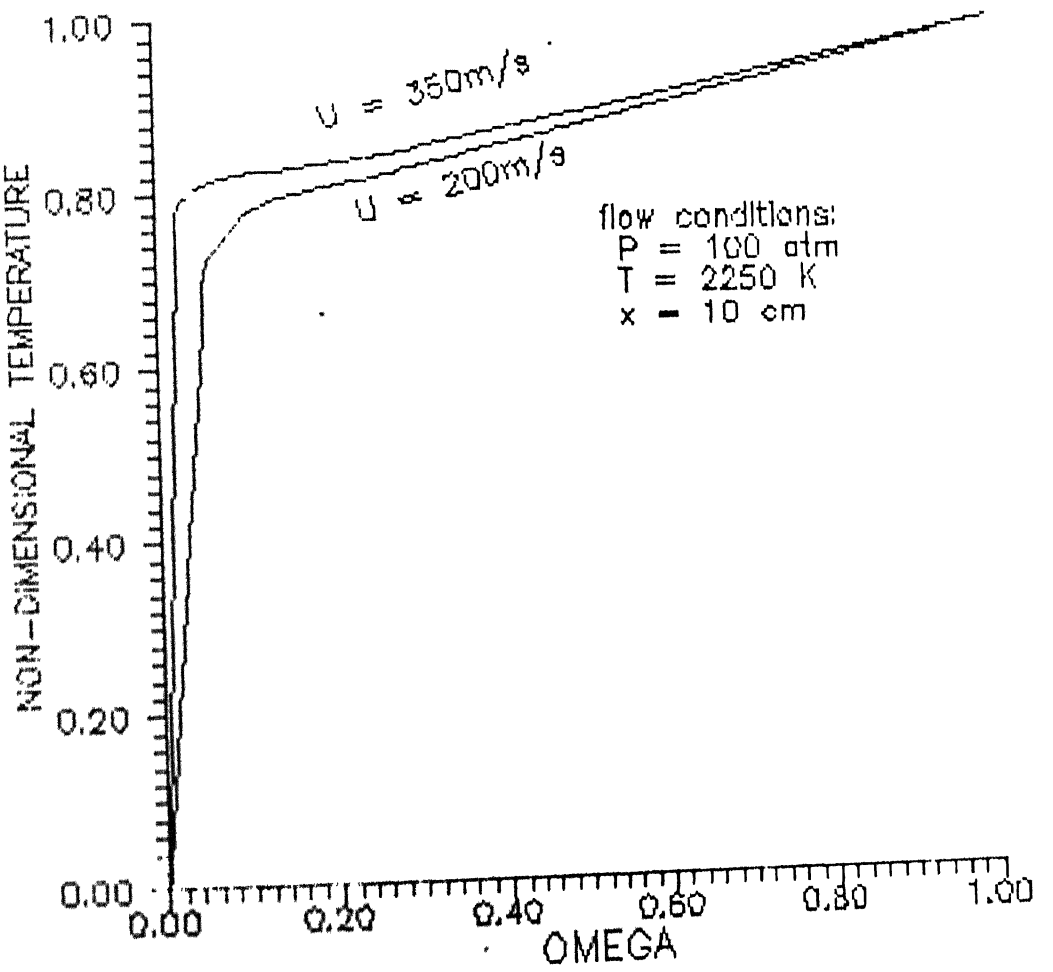

FIG 8 NON - DIMENSIONAL TEMPERATURE, $(T-T_{ps})/(T_{\infty}-T_{ps})$, PROFILE

reactions taking place there.Fig.9 shows the calculatd distributions of fuel and oxidiser mass fractions.It is evident from Fig.9 that fuel and oxidiser mass fractions drop to very small values near the propellant surface implying that chemical reactions are quite fast in that region and therefore,the rate of heat generation due to chemical reactions in gas phase also rises sharply from its zero value at the surface ,becoming maximum in the near-wall region and then gradually decreasing to zero at the freestream edge of the boundary layer(this is quite consistent with the temperature distribution shown in Fig.8).

It is also clear from Fig.8 that temperature gradient becomes steeper as the freestream velocity increases which means higher gas-to-solid heat flux.This fact is expected because higher freestream velocity induces higher turbulence intensity near the propellant surface.This causes an increase in the mixing rate of the oxidiser and fuel species and therefore gas-phase reaction rate increases.Thus we have a double-fold effect of increase in freestream velocity.firstly peak value of rate of heat generation due to chemical reaction increases and secondly the location of this peak value comes closer to the propellant surface.Both of these factors add to the gas-to-solid heat flux and thus makes the temperature gradient steeper in the near-wall region.

Another consequence of increase in freestream velocity is the higher total burning rate(see Fig.10) or increase in the erosive burning augmentation factor (r_b/r_{bo}) as shown in Fig.12.As discussed above the gas-to-solid heat flux rises with the freestream velocity which means that propellant

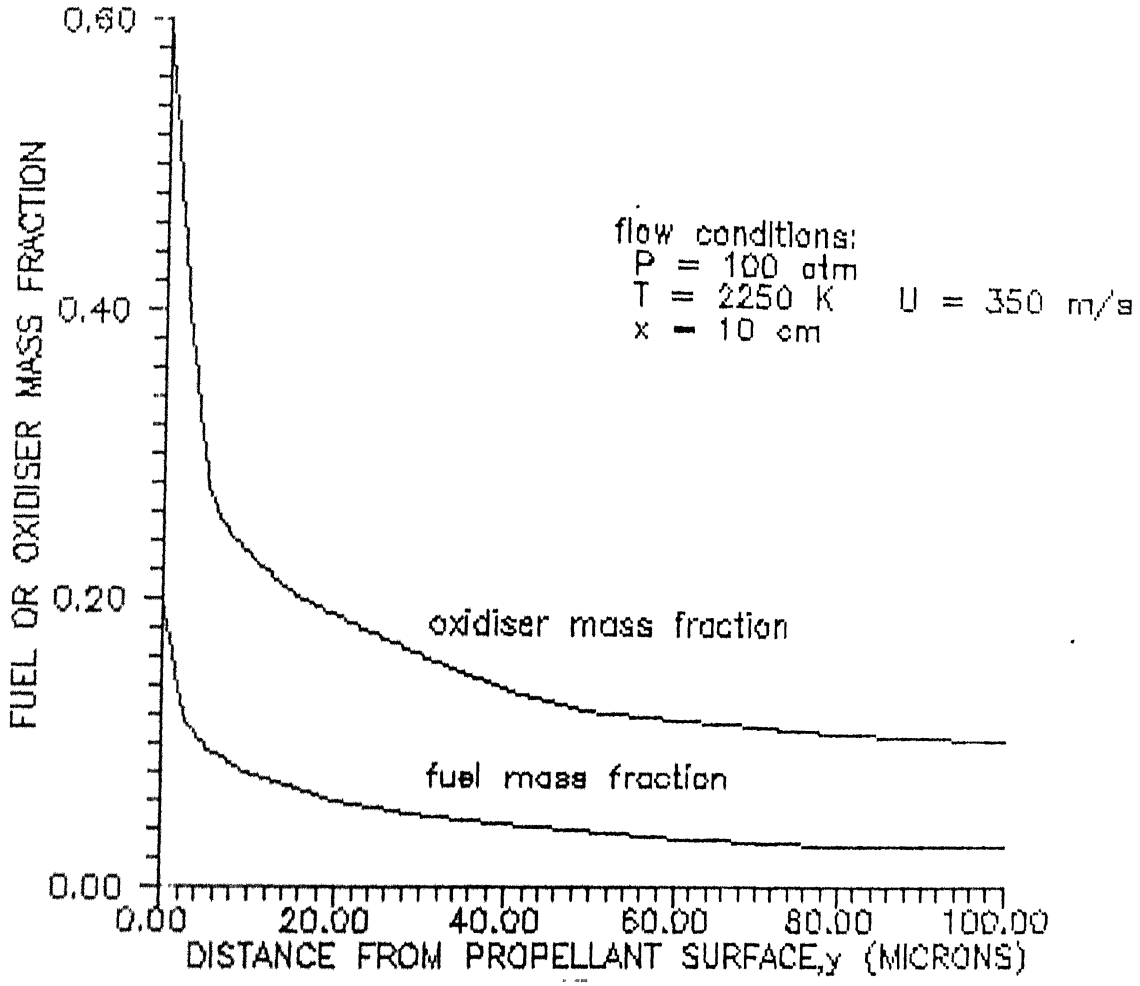

FIG.9 PROFILE OF FUEL AND OXIDISER MASS FRACTIONS

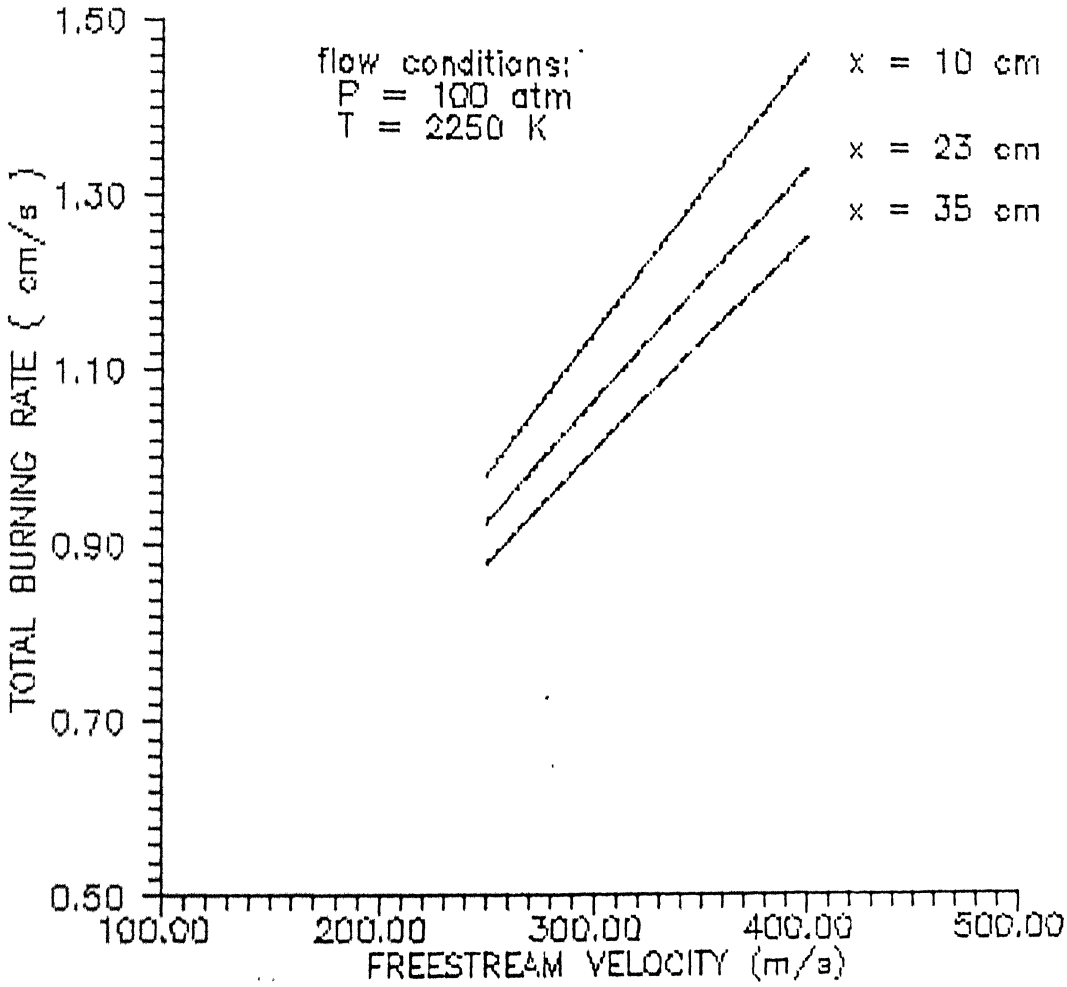

FIG.10 TOTAL BURNING RATE VS. FREE STREAM VELOCITY AT VARIOUS X - LOCATIONS

surface temperature increases,making its burning rate higher On extrapolation, a threshold velocity (below which there is no increase in burning rate) nearly equal to 200 m/s can also be noticed in Fig 12.

Fig 11 shows the variation in burning rate along the propellant surface It is observed that the burning rate decreases as one moves downstream This is brought about by the fact that the boundary layer is thin near the upstream end resulting in maximum gas-to-solid heat flux As one moves downstream , boundary layer thickness increases and reducing the gas-to-solid heat flux

In Fig 13 , the effect of surface roughness on the erosive burning augmentation factor for different freestream velocities is shown As the roughness height increases , the augmentation factor also increases This is due the fact that increased roughness height causes more turbulence activity near the propellant surface and therefore more mixing of fuel and oxidiser species Also the effect of roughness height is more pronounced at the higher freestream velocities.This is due the fact that at low freestream velocity , thickness of laminar viscous sublayer is more and submerges the roughness element But at higher freestream velocities , goes on becoming thin and roughness facor greatly influences the flowfield near the propellant surface.

Fig 14 shows the effect of normal burning rate (r_{bo}) on the erosive burning augmentation factor.The curve with normal burning rate equal to 0 69 cm/s is for AP/Polysulphide and the other curve with normal burning rate equal to 0.8 cm/s is for AP/PBAA/EPON propellant.It is observed that the propellant

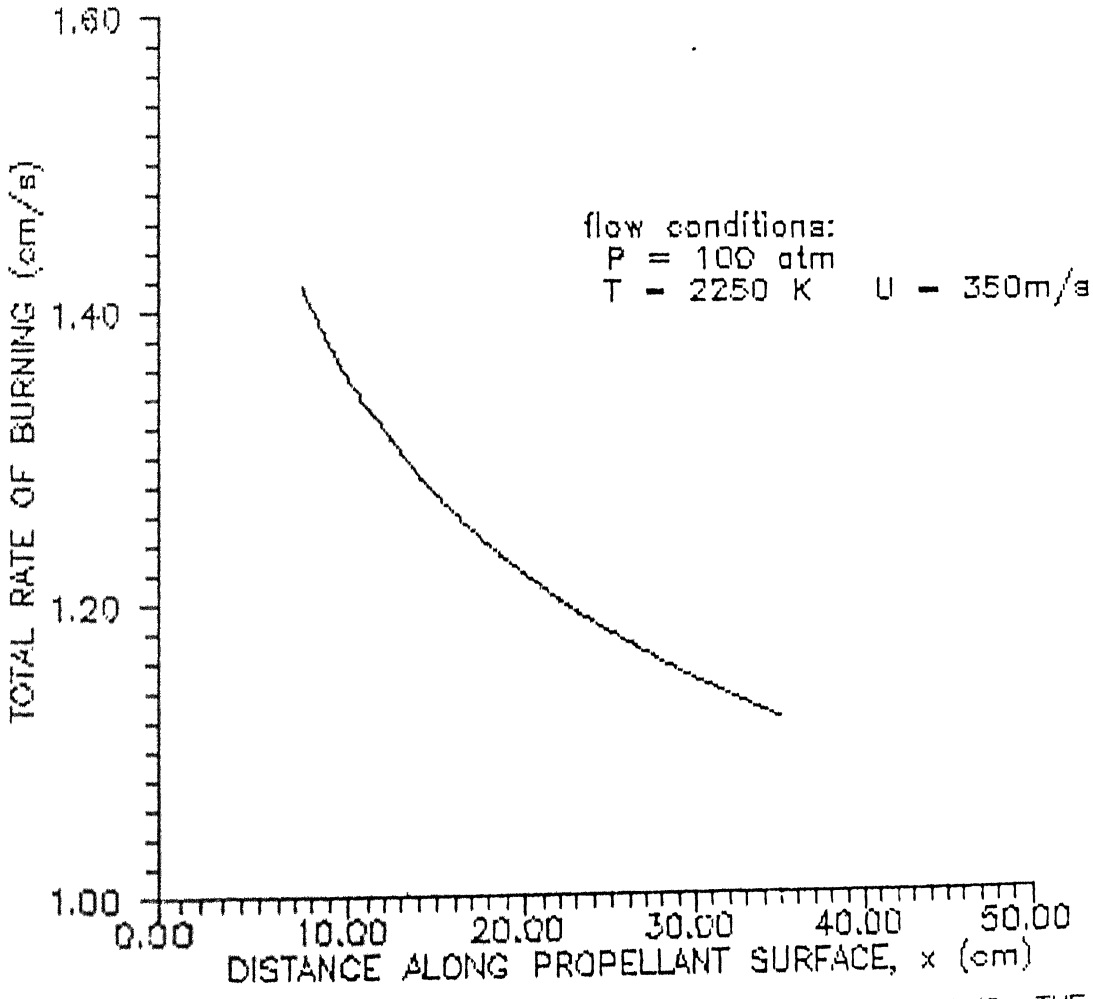

FIG.11 TOTAL BURNING RATE VS. THE DISTANCE ALONG THE PROPELLANT SURFACE

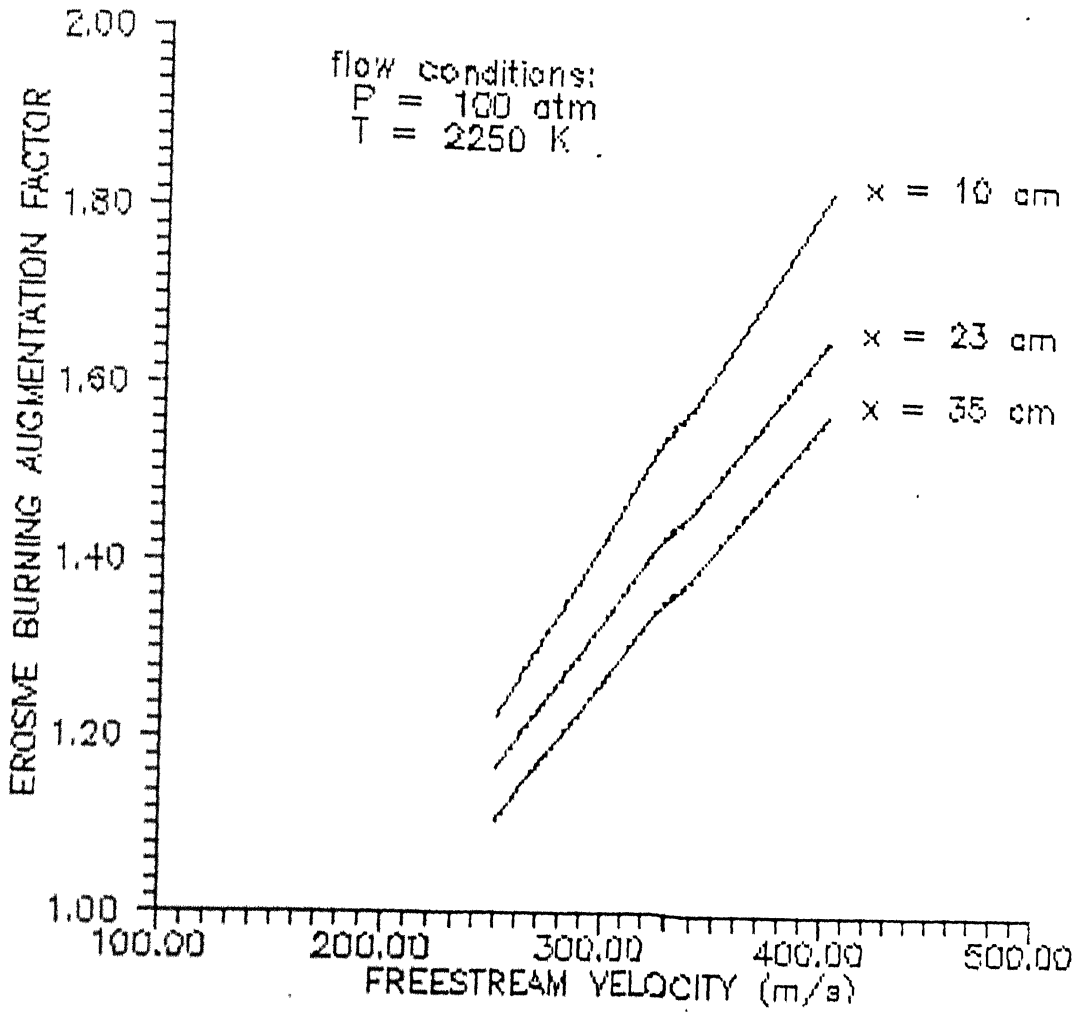

FIG 12 EROSIVE BURNING AUGMENTATION FACTOR VS FREE STREAM VELOCITY AT VARIOUS X - LOCATIONS

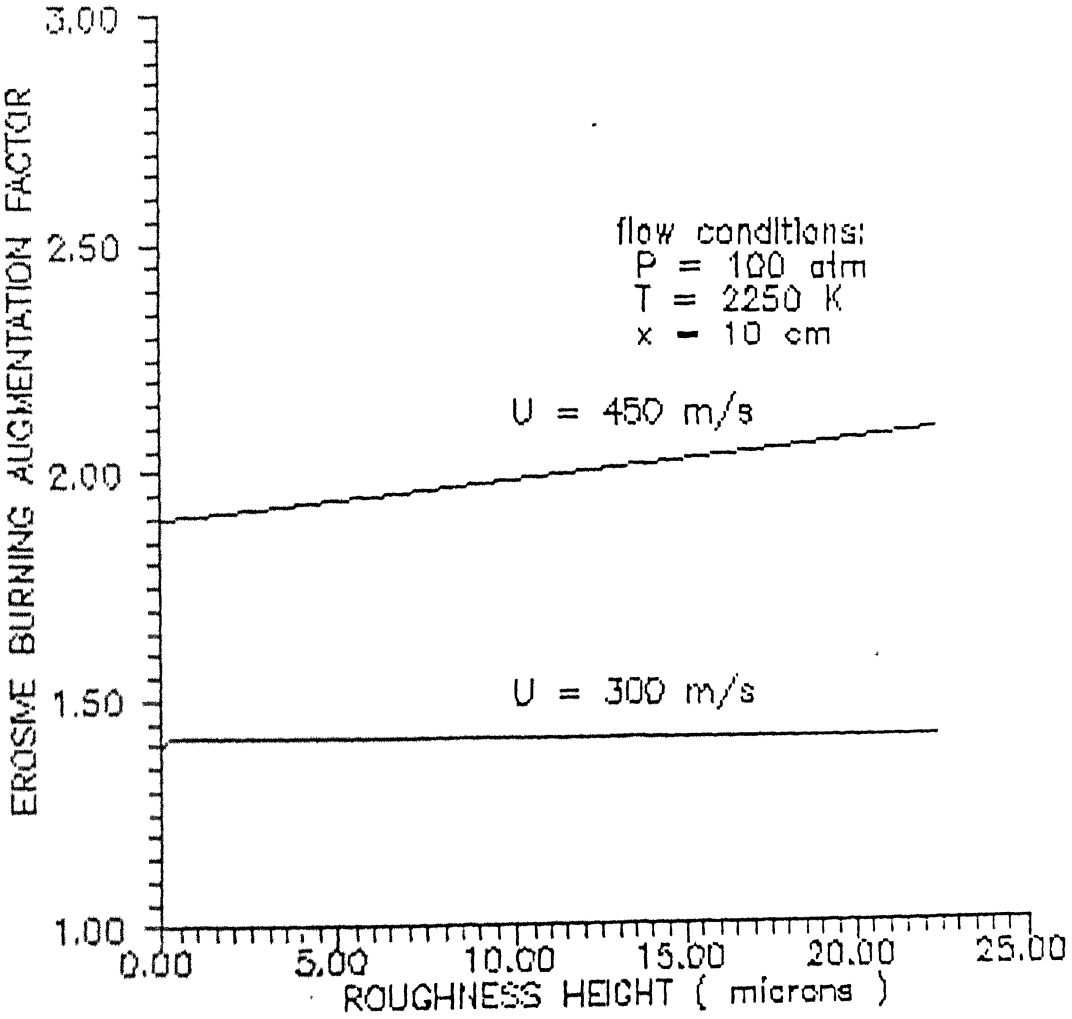

FIG.13 EFFECT OF SURFACE ROUGHNESS ON EROSIVE BURNING AUGMENTATION FACTOR AT DIFFERENT FREE STREAM VELOCITIES

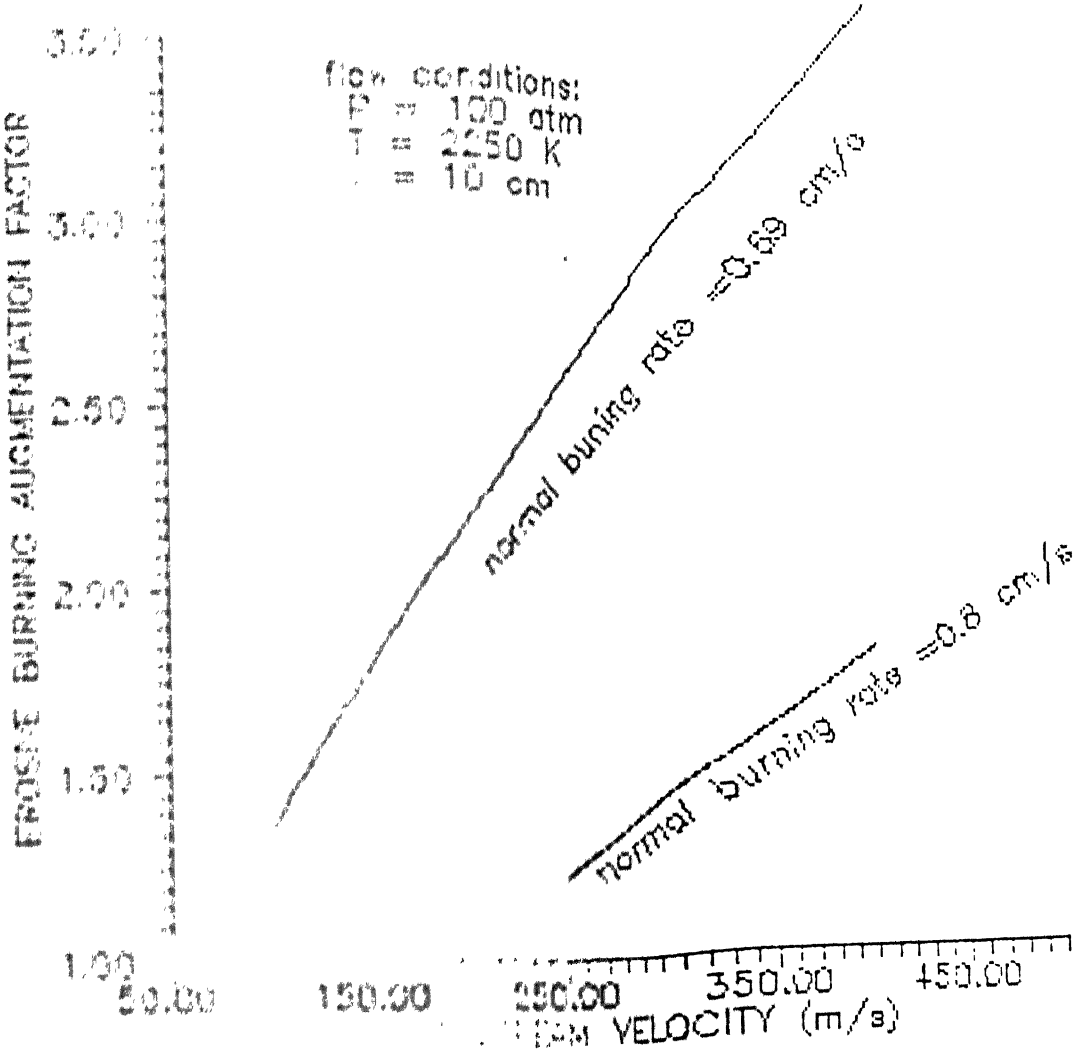

[illegible] EFFECT OF NORMAL [illegible] BURNING RATE ON THE EROSIVE BURNING
[illegible] FACTOR

with lower normal burning rate is more sensitive to the erosive burning effect than the propellant with higher normal burning rate.This can be attributed to the fact a fast burning propellant gives rise to thicker boundary layer over its surface due to higher crossstream mass flow rate than would be obtained in the case of a slow burning propellant.In the thicker boundary layer, there is less steep temperature gradient and lower gas-to-solid heat flux which results in lower erosive burning rate.

Also based on above discussion it can also be argued that as small particle size AP composite propellants have high normal burning rates , therefore they are less affected by crossflow.

(5 b) Conclusions

It is observed from the present calculations that freestream velocity greatly influences the burning rate of a composite propellant.Increase in freestream velocity increases the gas phase reaction rate and also brings the reaction zone closer to the propellant surface.The effect of roughness height is to increase the burning rate and this effect is more pronounced at higher free stream velocities.The propellants with lower normal burning rates are more sensitive to the erosive burning effect than the propellants with higher normal burning rates.

The present work can be easily extended to take into account the effect pressure gradient.Also the work can be modified for axisymmetric boundary layer , that is , to model the erosive burning problem of cylindrical

composite solid propellant.With the availability of more information about the chemical kinetics of the gas phase reactions , there is ample scope for modeling the reaction rate in a better way. For example, a combustion model based on multiple flames can be employed to have more accurate estimate of burning rate of composite propellant (see Ref 5).

Appendix A	References

Razdan, M.K. and Kuo, K.K ,"Erosive Burning of Solid Propellents."Fundamentals of Solid -Propellant combustion , edited by Kuo, K. K. and Summerfield, M., Progress in Astronautics and Aeronautics, Vol. 90, 1984, pp 515-598

. King, M. K.,"A Model of Erosive Burning of Composite Propellants,"J. Spacecraft, Vol. 15, No 3, May-June 1978, pp139-146

. Lenoir, J. M. and Robillard G,"A Method to Predict the Effects of Erosive Burning in Solid Propellant Rockets", 6th Symposium (International) on Combustion 1957, pp 663-667.

. Hermance, C.E, " A Model of Composite Propellant Combustion Including Surface Heterogeneity and Heat Generation", AIAA Journal, Vol. 4, No. 9 , Sept 1966, pp 1629-1637

. Beckstead, M. W., Derr, R. L. and Price, C. F., " A Model of Composite Solid-Propellant Combustion Based on Multiple Flames", AIAA Journal, Vol. 8, No 12, Dec 1970, pp 2200 - 2207

. Lengelle, G, " Model Describing the Erosive Combustion and Velocity Response of Composite Propellants ", AIAA Journal, Vol. 13, March 1975, pp 315-322.

. Beddini, R.A., " Reacting Turbulent Boundary - Layer Approach to Solid Propellant Errosive Burning", AIAA Journal, Vol. 16, No. 9, September, 1978, pp 898-905

. Razdan, M.K. and Kuo, K.K ,"Erosive Burning study of composite Solid Propellants, by Turbulent Boundary-Layer Approach ",AIAA Journal , Vol 17, No. 11, November

1979 pp 1225-1233

9 Penie, J P and Osborn, J R ," Erosive Burning ",AIAA Journal , Vol. 21, No. 12 , December, 1983. pp 1681-1688

10 Godon, J C., Duterque, J and Lengelle, G , "Solid Propellant Erosive Burning", 23 Ieme Conférence AIAA Sur la Propulsion, San-Diego, 29 juin - 2juillet 1987.

11 Sabnis, J S., Gibeling, H. J , and McDonald, H , " Navier-Stokes Analysis of Solid Propellant Rocket Motor Internal Flows", J. Propulsion, Vol 5, No. 6, Nov-Dec 1989 pp 657- 664.

12. Boggs, T L , Derr, R. L., and Beckstead, M W , " Surface Structure of Ammonium Perchlorate Composite Propellants", AIAA Journal , Vol 8. No. 2. Feb 1970, pp 370-372

13. Spalding, D B ,"Development of the Eddy-Break-Up Model of Turbulent Combustion",Numerical Prediction of Flow, Heat Transfer, Turbulence and Combustion edited by Patankar, S. V and others, Pergamon Press, pp 194-200

14 Cebeci T and Chang, K C., " Calculation of Incompressible Rough Wall Boundary Layer Flows" , AIAA Journal , Vol. 16, July 1978, pp 730-735

15 Van Driest, E. R ," On Turbulent Flow Near a Wall ", Journal of Aeronautical Sciences, Vol. 23, Nov 1956, pp 1007-1011

16. Launder, B E and Spalding D.B., " Numerical Prediction of Flow, Heat Transfer, Turbulence and Combustion ", edited by Patanker, S V and others, Pergamon Press, pp 96-116.

17. Singhal A K. and Spalding, D.B.,"Prediction of Two-Dimensional Boundary Layers with the Aid of the k-ε Model of Turbulence", edited by Patanker, S.V. and others, Pergamon Press, pp 411-429

Kuo, K.K., " Principles of Combustion", John Wiley & Sons (1986)

Lebedi, T and Smith, A.M.O., "Analysis of Turbulent Boundary Layers", Academic Press, 1974

Patankar, S.V. and Spalding, D.B.," Heat and Mass Transfer in Boundary Layers", Inter-Text Books, London, 1970

Spalding, D.B., " GENMIX : A General Computer Program for Two-Dimensional Parabolic Phenomena" , Pergamon Press, 1977.

Appendix B	Physical Constants

The values of the physical constant used are indicated below :

A_s	=	2E174	
C_P	=	0.3	kcal / kg-K
C_s	=	0.38	kcal / kg-K
E_{as}	=	30	kcal / mole
P	=	100	atmosphere
Pr	=	0.7078	
Pr_t	=	0.9	
Q_s	=	−166	kcal / kg
R_u	=	1.98	kcal / kmole ^{0}K
Sc	=	0.7078	
Sc_t	=	0.9	
T_∞	=	2250	K
T_{Pi}	=	298	K
$\bar{T}_{ps}$	=	800	K
W_F	=	30	kg / mole
W_O	=	27.8	kg / mole
ν_F	=	1	
ν_O	=	3.2266	
ρ_s	=	1600	kg / m^3
C_1	=	1.0	
C_2	=	1.3	

C_3 = 1.57

C_4 = 2.0

C_ω = 0.18

C_μ = 0.09

C_ρ = 1.0

Appendix C | Flow Diagram And Its Description

Fig 15 shows the flow diagram of the solution procedure. What various subroutines do, is described below in brief.

1 MARCH_START

(i) Reads the input data

(ii) Sets the initial profiles of flow variables except k and ε

2 PHY_PROPERTIES .

(i) Sets the initial profiles of k and ε

(ii) Calculates the value of various physical properties, μ , μ_t , ρ etc. at all the grid points.

3 ENTRAINMENT_RATE

(i) Mass flow rates at I and E boundaries are calculated

4 READY .

(i) Calculates Y-distances between the grid points

(ii) Sets the step size, if next step is to be taken

(iii) Sets the initial (guess) wall values at the downstream location

5 WALL_REGION

(i) Wall functions are calculated.

6 SOURCE.

(i) Calculates the value of S_i and S_i' for all the conservation equations and at each grid point

7 SOLVE .

(i) Tri-diagonal system of algebraic system of equation is solved.

8 CORE-REGION

(i) The coefficients A_p, B_p, etc. for each conservation equation are calculated

(ii) Calls the WALL-REGION, SOURCE and SOLVE to give the value of flow variable at the downstream location

9 CONVERGENCE :

(i) The wall boundary condition are checked and iteration is done till they are satisfied.

10 STEP-OUTPUT :

(i) Writes the output of the program at a x-location

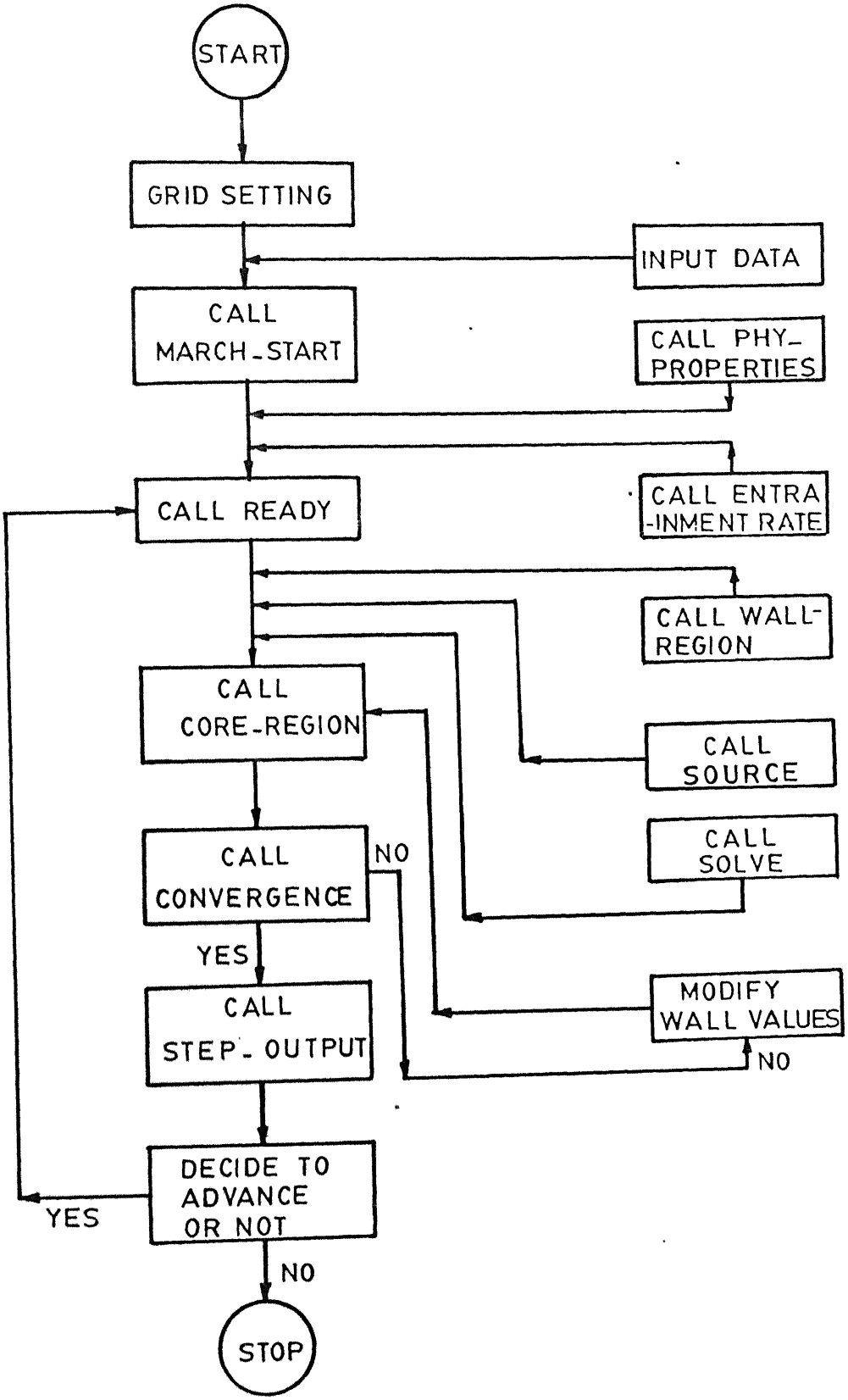

FIG. 15 FLOW DIAGRAM OF THE SOLUTION PROCEDURE